SANDIA REPORT
SAND2021-8143
Printed July 2021

Sandia National Laboratories

Suitability of Altair FEKO's Computational Electromagnetic Techniques for Tree Model Scattering and Penetration at Ku-band

Monica R. Jaramillo
Armin W. Doerry
Christos G. Christodoulou (The University of New Mexico)

Prepared by
Sandia National Laboratories
Albuquerque, New Mexico
87185 and Livermore,
California 94550

Issued by Sandia National Laboratories, operated for the United States Department of Energy by National Technology & Engineering Solutions of Sandia, LLC.

Available to DOE and DOE contractors from
U.S. Department of Energy
Office of Scientific and Technical Information
P.O. Box 62
Oak Ridge, TN 37831

Telephone: (865) 576-8401
Facsimile: (865) 576-5728
E-Mail: reports@osti.gov
Online ordering: http://www.osti.gov/scitech

Available to the public from
U.S. Department of Commerce
National Technical Information Service
5301 Shawnee Rd
Alexandria, VA 22312

Telephone: (800) 553-6847
Facsimile: (703) 605-6900
E-Mail: orders@ntis.gov
Online order: https://classic.ntis.gov/help/order-methods/

ABSTRACT

Foliage penetration (FOPEN) radar at lower frequencies (VHF, UHF) is a well-studied area with many contributions. However, there is growing interest in using higher Ku-band frequencies (12-18 GHz) for FOPEN. Specifically, the reduced wavelength sizes provide some key saliencies for developing more optimized detection solutions. The disadvantage is that exploiting Ku-band for FOPEN is complicated because higher frequencies have pronounced scattering effects due to their smaller wavelengths.

A methodology has been developed to model and simulate FOPEN problems that characterize the phenomenology of Ku-band electromagnetic (EM) wave transmissions through moderate foliage. The details of this research (i.e. the realistic tree models, simulation setup and results) are documented in multiple reports. The main focus of this report is to describe the preliminary validation and verification of Altair FEKO, the computational EM (CEM) software used for this research, as well as present a simplified symmetrical tree model and an introductory CAD tree model.

ACKNOWLEDGEMENTS

This report was funded in part by General Atomics Aeronautical Systems, Inc. (GA-ASI) Mission Systems under Cooperative Research and Development Agreement (CRADA) SC08/01749 between Sandia National Laboratories and GA-ASI.

General Atomics Aeronautical Systems, Inc. (GA-ASI), an affiliate of privately-held General Atomics, is a leading manufacturer of Remotely Piloted Aircraft (RPA) systems, radars, and electro-optic and related mission systems, including the Predator®/Gray Eagle®-series and Lynx® Multi-mode Radar

This study is in partial fulfillment of a Ph.D. dissertation research at the University of New Mexico (UNM) under the advisement of Dr. Christos Christodoulou with additional technical help from Dr. Armin Doerry.

The authors would also like to acknowledge and thank SNL manager, Matt Lewis for the support and for creating the opportunity for this research.

Additional heartfelt thank you to the whole SNL Common Engineering Environment (CEE) team for the dedicated technical computing resources, support and guidance.

Furthermore, great appreciation for Josh Pennington, Smit Baua and many of the other Altair Engineers that dedicated so much time, and attentively provided excellent Altair software technical support that allowed for this research to develop to full potential.

An extra special thank you to Dr. Ann Marie Raynal for taking personal time to review this report and provide excellent and knowledgeable advice.

CONTENTS

LIST OF FIGURES

ACRONYMS AND DEFINITIONS

Abbreviation	Definition
CAD	computer-aided design
CEM	computational electromagnetics
EM	electromagnetics
FEKO	feldberechnung für körper mit beliebiger oberfläche
FOPEN	foliage penetration
HH	horizontal horizontal
MLFMM	multilevel fast multipole method
PEC	perfect electric conducting
RCS	radar cross section
SAR	synthetic aperture radar
SLICY	Sandia Laboratories implementation of cylinders
UHF	ultra high frequency
VV	vertical vertical
VHF	very high frequency

FOREWORD

This report details the results of an academic study. It does not presently exemplify any modes, methodologies, or techniques employed by any operational system known to the authors.

Classification

This report formalizes preexisting informal notes and other documentation on the subject matter herein.

This report has been reviewed and approved to be Unclassified – Unlimited Release

Contact Information

Monica Jaramillo monjara@sandia.gov (505) 845-0051

1. INTRODUCTION

Synthetic aperture radar (SAR) remote sensing of foliage is crucial to many commercial and military application scenarios such as terrain mapping, biome characterization, human/object detection for search and rescue, vehicular tracking, boarder surveillance, wireless communication channel modeling, etc. Some of the key tasks include discriminating foliage in mapped terrains, identifying forest types, discerning tree heights, and detecting anomalies or hidden objects beneath foliage. The interaction of transmitted electromagnetic (EM) waves with foliage, especially penetrating the foliage canopy, is termed FOPEN (FOliage PENetration) [1], [2]. The characterization of EM wave interactions with any generic object is a complex multi-faceted problem that must take into account a range of parameters relating to the object type and application scenario. By extension, the more specialized FOPEN case presents further challenges since foliage acts as a dielectric material which can scatter, reflect, diffract, refract and attenuate impinging EM waves, from anywhere within its volume. In addition, related scattering and attenuation effects are much more pronounced at higher transmission frequencies.

Foliage scattering at lower frequencies (UHF, VHF) is a well-studied area with a wide set of contributions to date. Nevertheless, there is growing interest in using higher Ku-band frequencies for FOPEN analysis, i.e., 12-18 GHz transmission range. In particular, the reduced wavelength sizes (in the centimeters range) provide some key saliencies for developing more optimized foliage mapping solutions. Foremost, compact Ku-band antenna designs can yield sizeable space and weight savings. For this reason, the Ku-band has become a popular operating band for many unmanned aerial systems (UAS) [3]. Furthermore, system designers can also achieve finer scan resolution via the Ku-band, helping improve overall foliage characterization and detection capabilities.

Quantifying the interaction of foliage with EM frequencies in the Ku-band, overall, remains largely unaddressed in the modeling realm today. It is reasonable to expect that foliage transmissivity involves complicated scattering internal to the canopy, necessitating a modeling tool's ability to accurately deal with complicated scattering environments. Consequently, this problem requires tree and foliage models to have a high degree of fidelity, so much so as to severely tax the current available computing resources. These limitations of available computing resources also severely limit the data generation abilities, demanding judicious choices in parameter selection. All of this led to a research project for laying out a methodology to model and simulate FOPEN problems that characterizes the phenomenology of Ku-band EM wave transmissions through moderate foliage. The details of this project (i.e. the realistic tree models, simulation setup and results) are provided in [4], [5], [6] and [7].

The main focus of this report deals with validation of Altair FEKO [8] as a tool to ultimately address the part of this overall research problem that is the transmissivity through a foliage canopy. The validation strategy is to assess FEKO's ability to provide accurate scattering measurements from a succession of targets. In particular, simulation

results from different articles were first used for verification of FEKO implementation. Simple canonical and complex objects modeled in these articles were reconstructed in FEKO, and the results were successfully replicated with very good agreement. Also, measured data of a simple canonical object was used for validation, and the FEKO results agreed well with the measured data. This verification process was then expanded to a symmetrical tree model. Different material and scene scenarios with this symmetrical tree model were implemented and the results all concurred with the expectations of electromagnetic physics. Furthermore, a computer-aided design (CAD) tree model was created and implemented to replicate results from an article. Several different FEKO solution methods were considered for each problem and the method most appropriate for each model was employed.

2. MODEL VERIFICATION WITH SIMPLE CANOINCAL OBJECTS

The first model considered was a dielectric sphere in free space presented by [9]. The authors used a method called Volume-Element-Free Scheme (VEFS). The sphere radius is 0.32λ with a permittivity of 3.75. The frequency considered is 300 MHz with an incident plane wave source where theta = 0º and phi = 0º. The results obtained are bistatic Radar Cross Section (RCS) with theta = 0º - 180º; increment of 1º, and phi = 0º for a polarization of vertical vertical (VV) and horizontal horizontal (HH). When replicating the results, the solver utilized was MoM because of the low frequency and the electrically small sphere. A side by side comparison and an overlay of the results obtained in FEKO and the results from the article are shown in Figure 1 (a) – (c). The results agree very well for both the VV and HH polarization and are within 0.25 dBsm over the entire angle range.

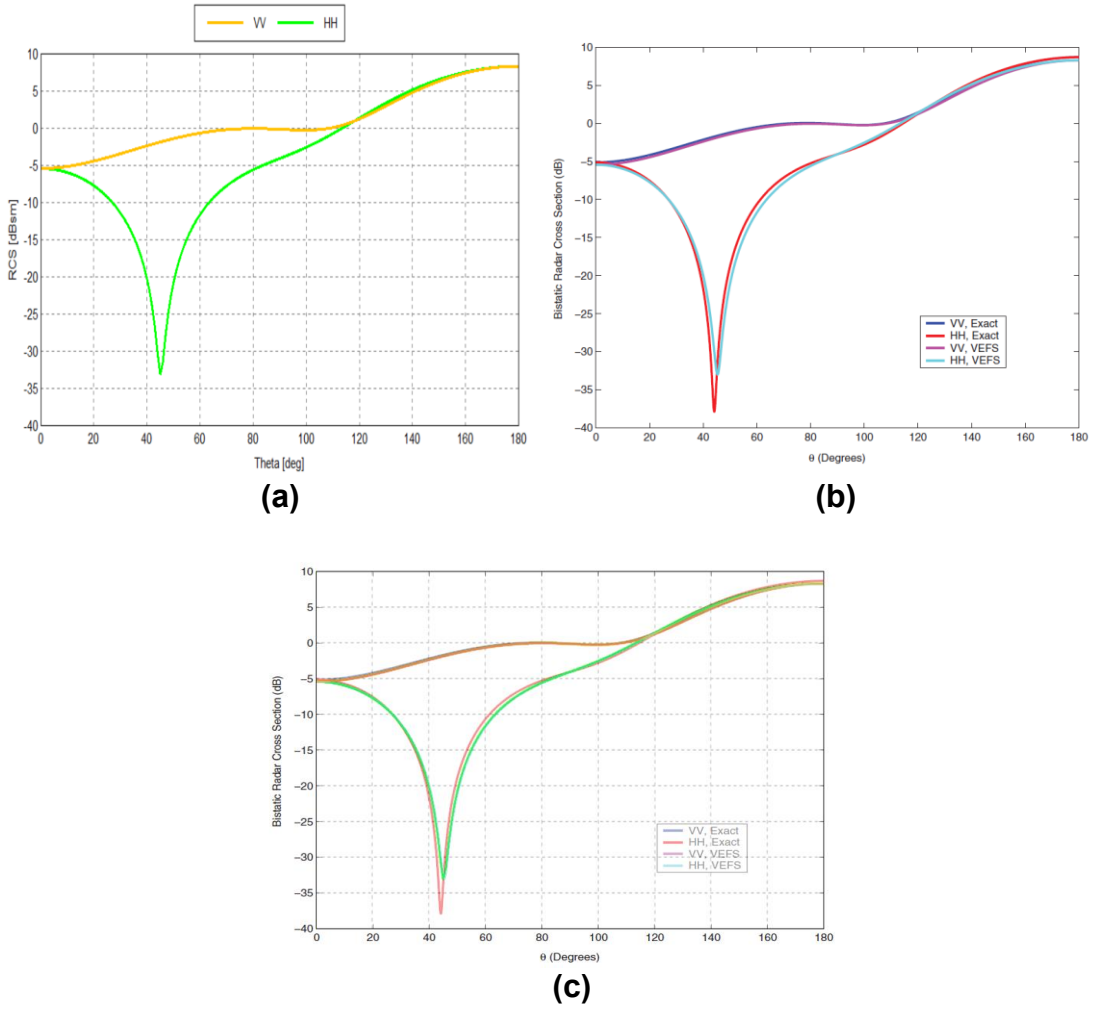

Figure 1: Bistatic VV and HH RCS (dBsm) results from a dielectric sphere: (a) FEKO results, orange line (VV) and green line (HH); (b) article [9] results, dark blue and purple lines (VV) and red and light blue lines (HH); (c) FEKO results overlaid on the article results.

Another model replicated was a perfect electric conducting (PEC) sphere model in free space from [10]. The method used in the article is a mixed-form fast multipole algorithm (Mixed-form (FMA)). The PEC sphere has a radius of 1 m, the frequency is 0.24 GHz and the source is an incident plane wave with theta = 0º and phi = 0º. The bistatic RCS is calculated for theta = 0º - 180º; increment of 1º, and phi = 0º with a polarization of VV. Multilevel fast multipole method (MLFMM) is the optimal method for the replicated simulation because of the size of the sphere. The results solved with FEKO and the results from the article are shown in Figure 2 (a) – (c), and are well matched over the entire angle span with no more than a displacement of 0.001 dBsm.

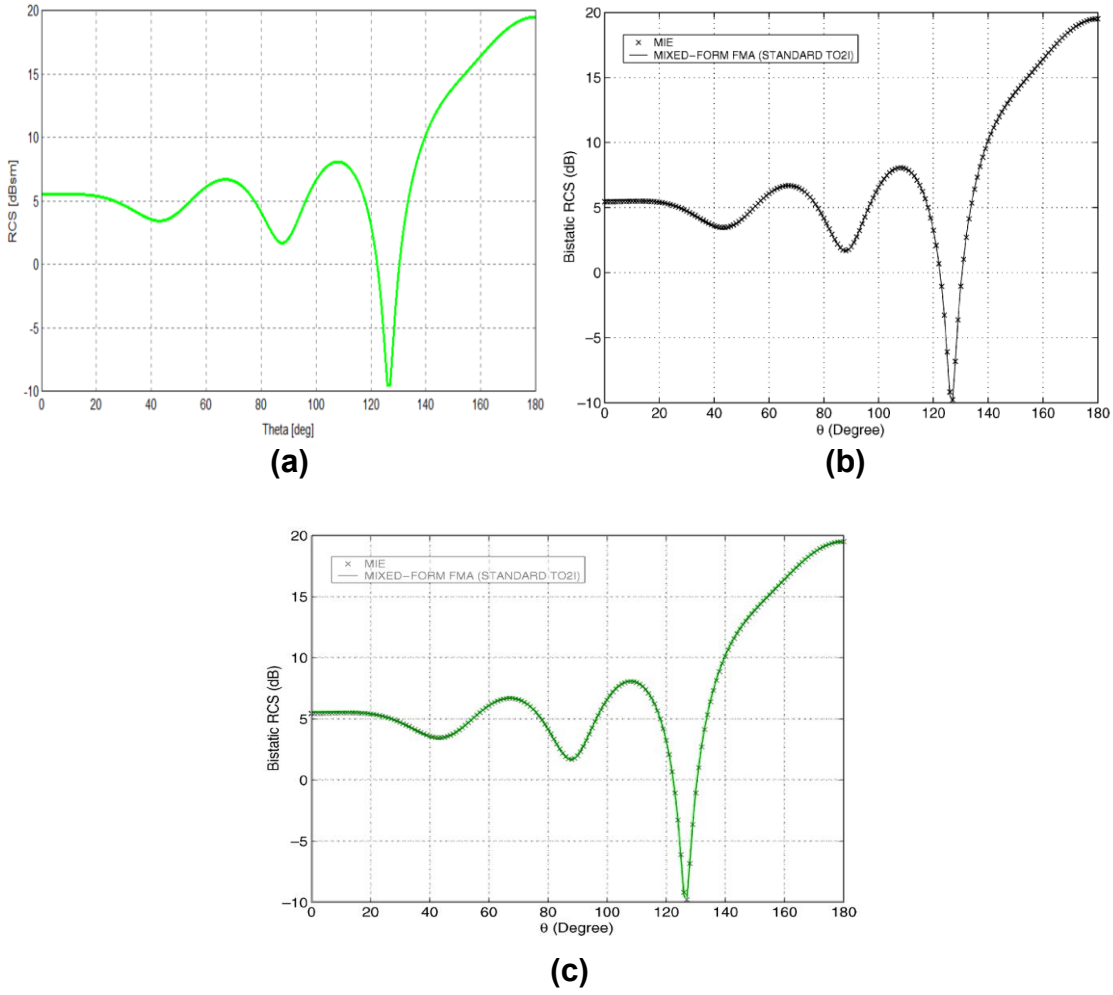

Figure 2: Bistatic VV RCS (dBsm) results from a PEC sphere: (a) FEKO results, green line; (b) article [10] results, black line and black X; (c) FEKO results overlaid on the article results.

A PEC cube and a dielectric sphere modeled in [11] were replicated. For the PEC cube, the authors compare several MoM-discretizations: Electric-Field Integral Equation

(EFIE) with Rao-Wilton-Glisson (RWG) basis functions, Electric-Magnetic Field Integral Equation (EMFIE) with divergence-Taylor-Orthogonal (div-TO) basis functions, Magnetic-Field Integral Equation (MFIE) with RWG basis functions and MFIE with div-TO basis functions. The diameter of the cube is 0.2 m, the frequency is 300 MHz, the model is meshed with 588 triangles and the source is an incident plane wave with theta = 0º and phi = 0º. The total bistatic RCS is calculated in the yz-plane with theta from 0º – 90º; increment 2º, and phi = 90º with a polarization of VV. The method used to reproduce this problem was MoM because of the low frequency. Note, the FEKO model was meshed with 576 triangles. Figure 3 (a) – (c) display the results.

As for the dielectric sphere solved in this article, since it is penetrable material, the MoM-discretization analyzed are Poggio-Miller-Chang-Harrington-Wu-Tsai (PMCHWT) with RWG basis functions, Muller with RWG basis functions, Muller with ORT1 and Mueller-EMME (Electric-Magnetic-Magnetic-Electric) with ORT1. The sphere radius is 0.1 m with a relative permittivity of 2, meshed with 128 triangles and the simulation parameters are the same as for the PEC cube. Note, the FEKO model was meshed with 126 triangles. The comparison total RCS results are in Figure 4 (a) – (c) and the FEKO model results are within less than 0.01 m^2 of the EFIE [RWG] results from the article.

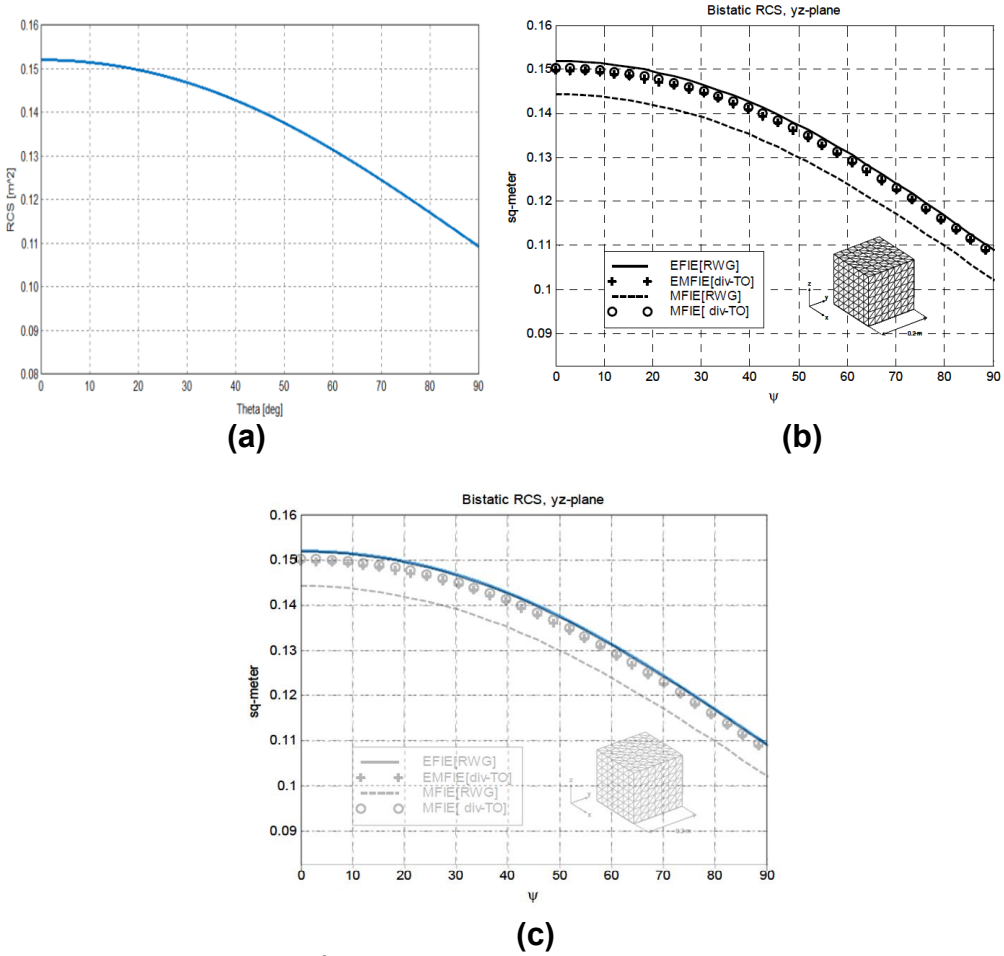

Figure 3: Total bistatic VV RCS (m^2) results from a PEC cube: (a) FEKO results, blue line; (b) article [11] results, all black lines; (c) FEKO results overlaid on the article results.

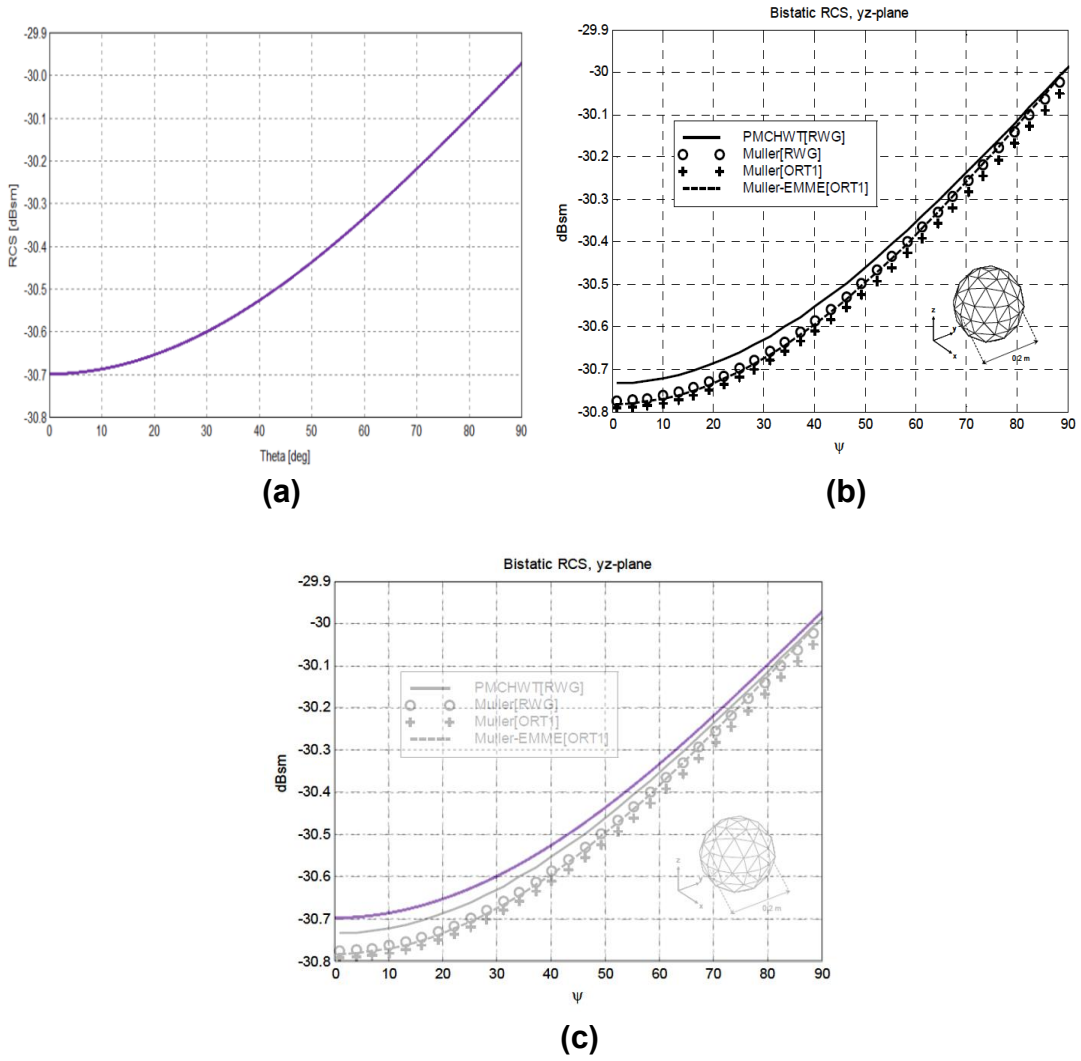

Figure 4: Total bistatic VV RCS (dBsm) results from a dielectric sphere: (a) FEKO results, purple line; (b) article [11] results, all black lines; (c) FEKO results overlaid on the article results.

A dielectric cube was solved using RL-GO because of the high simulation frequency. The parameters used were from two different articles [12], [13] that both modeled a dielectric cube with a length of 0.12 m, a dielectric constant of 2.7 - j0.01 and solved at a frequency of 30 GHz. The authors in [12] used GO to calculate the monostatic RCS with an incident plane wave where theta = 90º and phi = 0º - 45º using an increment of 0.1º. They simulated both polarizations, i.e. VV and HH. The results from [12] as well as the replicated FEKO results are shown in Figure 5 (a) – (c) for VV polarization and Figure 6 (a) – (c) for HH polarization. There is a slight mismatch in the results for VV polarization around 5º – 30º, and 5º – 32º for the HH polarization results. This is due to the different solvers used and is also displayed amongst the different solvers used within the article.

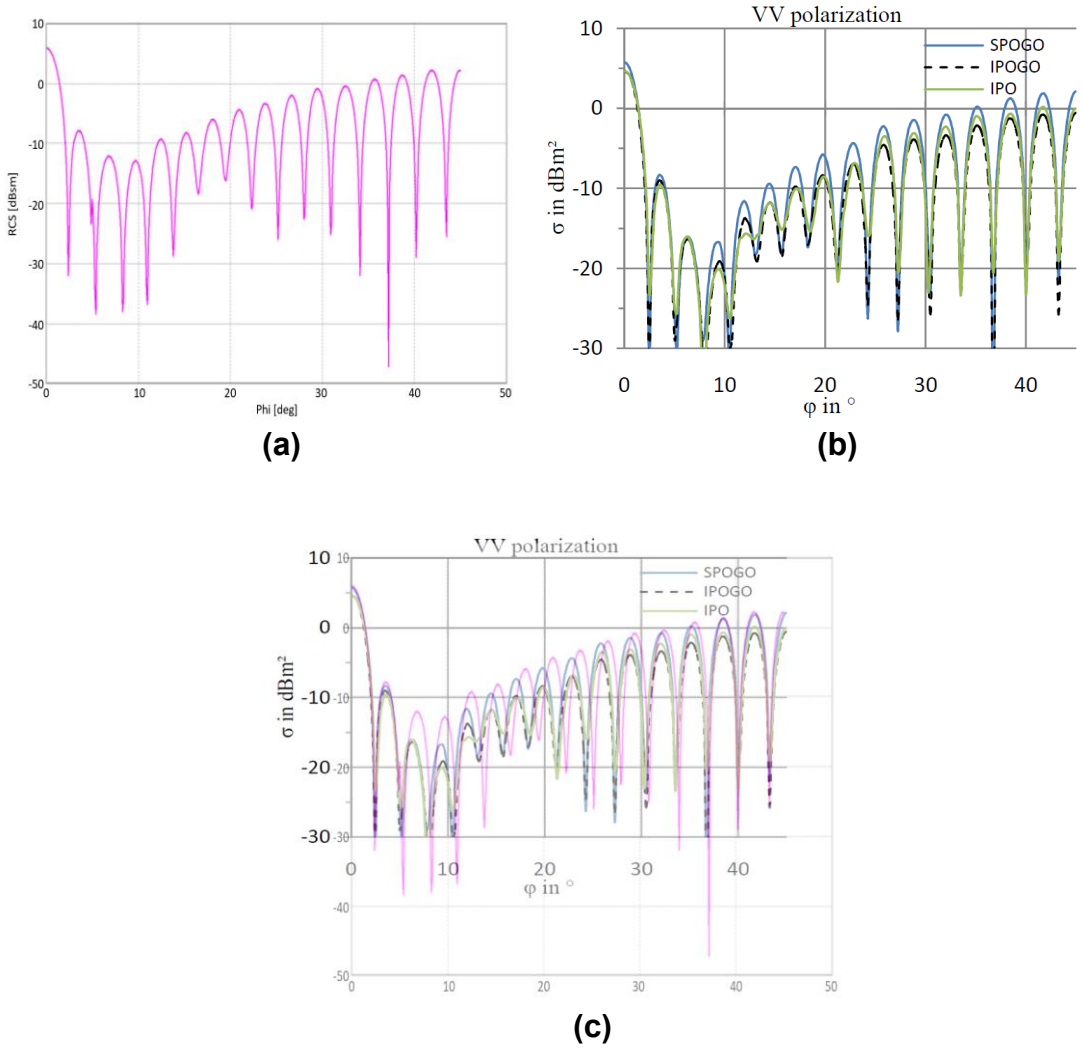

Figure 5: Monostatic VV RCS (dBsm) results from a dielectric cube: (a) FEKO results, pink line; (b) article [12] results, blue line, black dashed line and green line; (c) FEKO results overlaid on the article results.

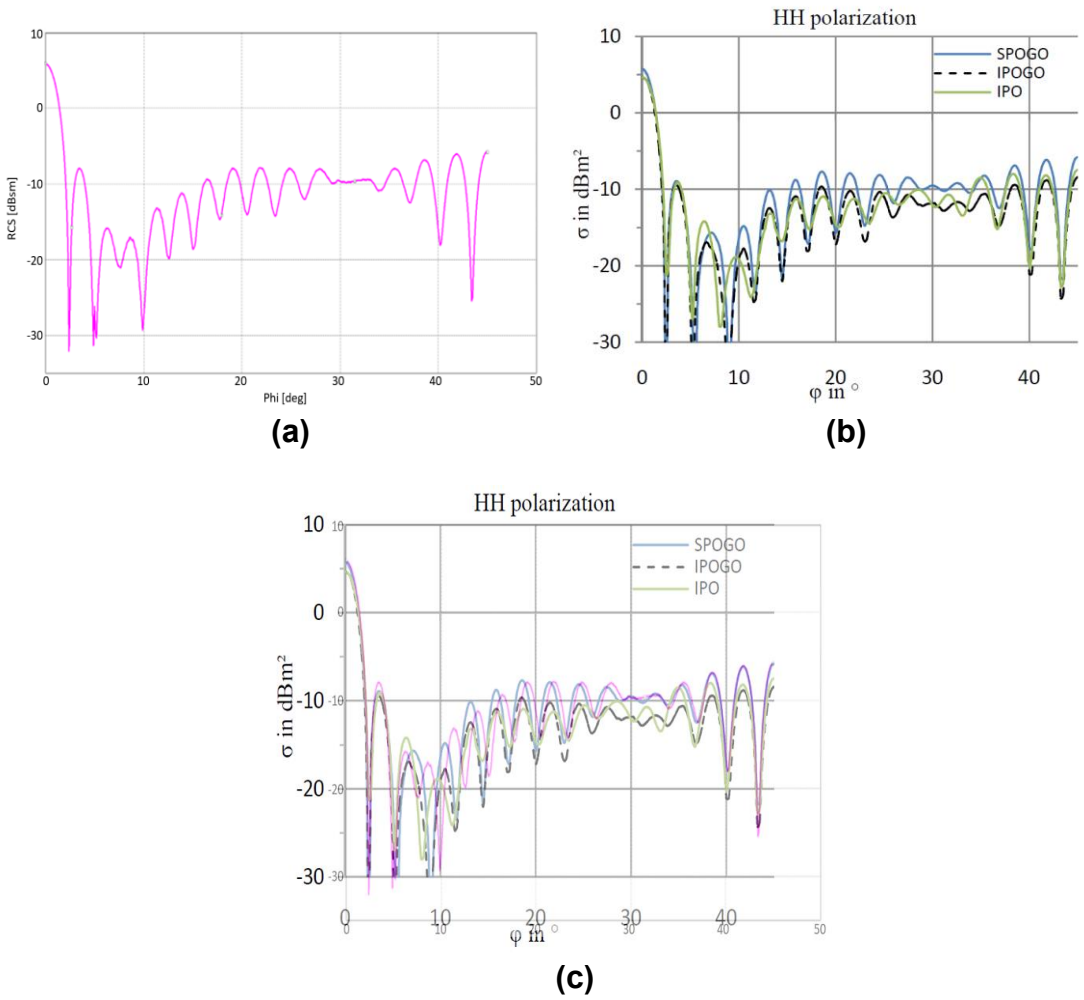

Figure 6: Monostatic HH RCS (dBsm) results from a dielectric cube: (a) FEKO results, pink line; (b) article [12] results, blue line, black dashed line and green line; (c) FEKO results overlaid on the article results.

As for the simulation of the dielectric cube in [13], the source setup is slightly different having an incident plane wave of theta = 90º and phi = 0º - 90º using an increment of 0.1º. In this article, the method used a ray-density normalization (RDN) with PO and physical theory of diffraction (PTD). They provided measured and simulated monostatic RCS data for both VV and HH. Figure 7 (a) - (c) display the results of the FEKO simulation compared to the measured data in the article [13] and Figure 8 (a) – (c) show the comparison of the FEKO simulated results to the simulated results in [13]. The FEKO simulated data, as well as the simulated data from the article have a similar trend as the measured data, however, there is not a complete match, and as articulated from the article, this difference is due to the simulated results being very sensitive because of the real and imaginary part of the relative permittivity value. Also, there may have been some measurement errors because of inaccurate positioning of the dielectric cube.

Regarding the slight offsets between the FEKO simulated results and the simulated results from the article, this is likely due to the different types of solvers used to calculate the RCS values.

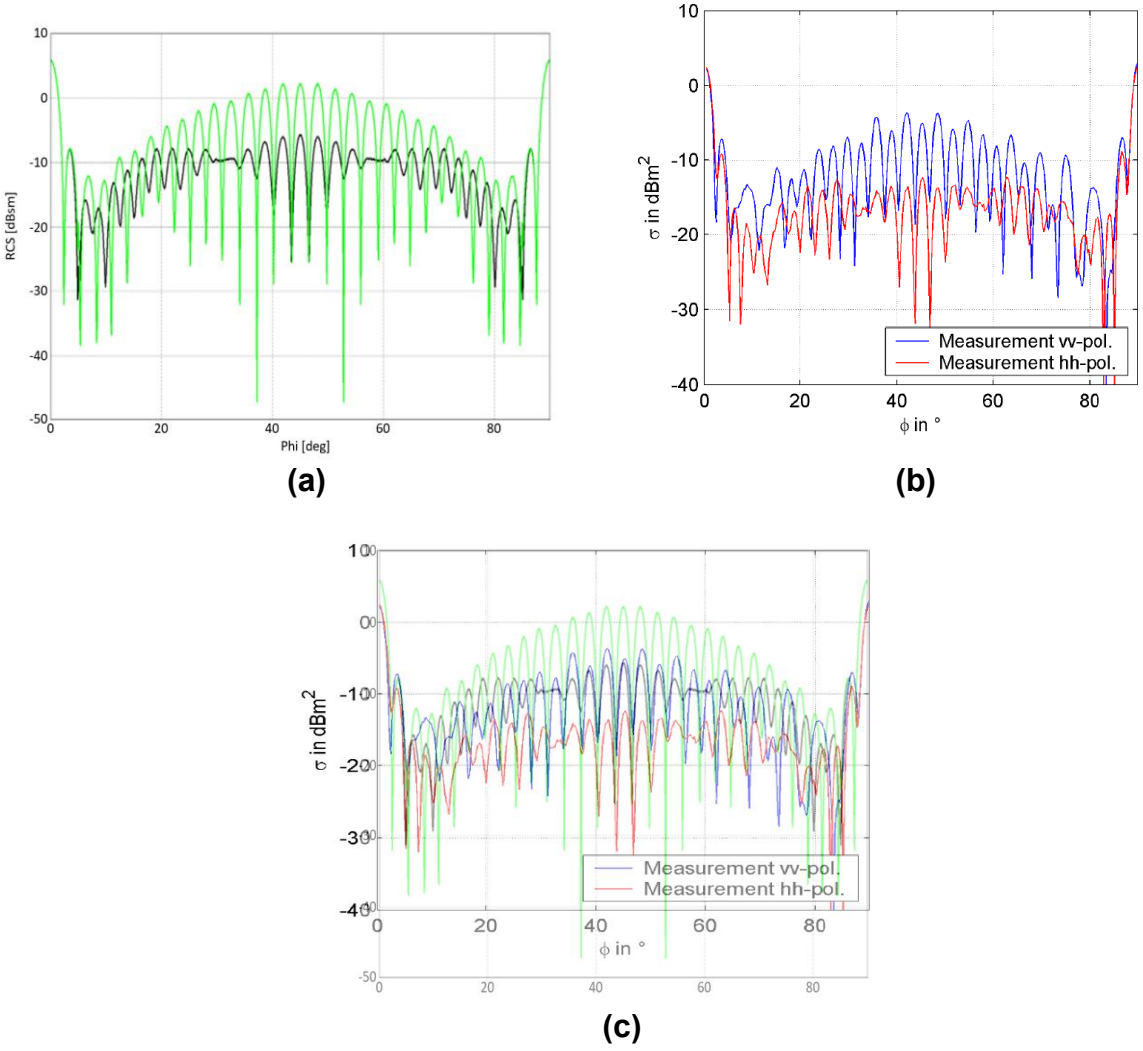

Figure 7: Monostatic VV and HH RCS (dBsm) results from a dielectric cube: (a) FEKO results, green line (VV) and black line (HH); (b) article [13] measured results, blue line (VV) and red line (HH); (c) FEKO results overlaid on the article measured results.

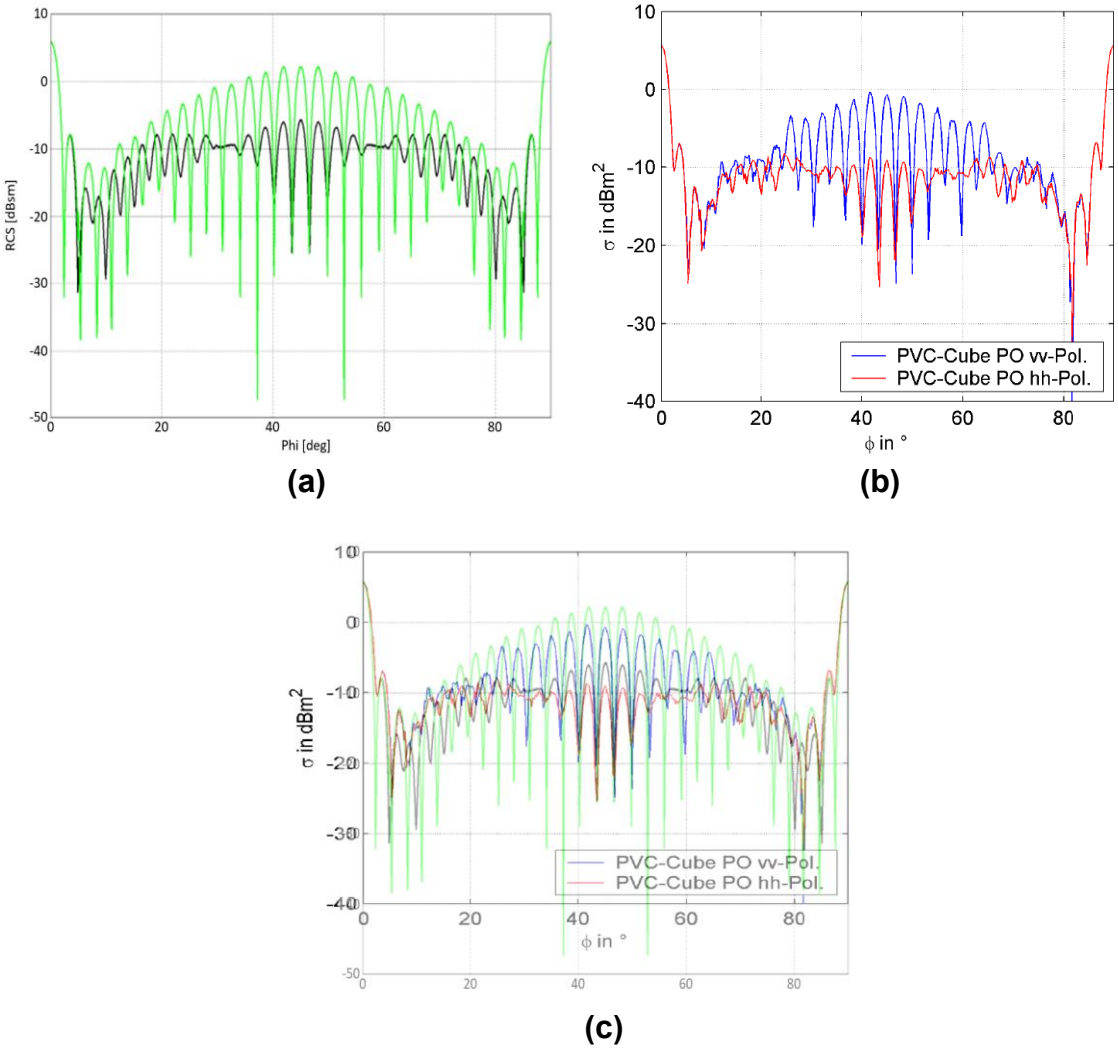

Figure 8: Monostatic VV and HH RCS (dBsm) results from a dielectric cube: (a) FEKO results, green line (VV) and black line (HH); (b) article [13] simulated results, blue line (VV) and red line (HH); (c) FEKO results overlaid on the article simulated results.

Two other models simulated was a coating plate and sphere that were modeled in [14]. The authors in the article used FEKO to simulate a full scale model, a theoretical model and a designed model. Both of the theoretical and designed models are 1/5 of the full scale model. The results obtained for all the models are transverse electric (TE) monostatic RCS with an incident plane wave theta = 0º - 90º; increment of 1º, and phi = 0º. All the coating plates and spheres have a coating permittivity of 14.49 - j0.12 and permeability of 3.56 - j1.12 with a bottom PEC face for the plates and a PEC core for the spheres. The frequency is 2 GHz for the full scale models and 10 GHz for the theoretical models. The full scale plate has a length = 0.5 m, width = 0.5 m and coating thickness = 0.002 m. The theoretical plate has length = 0.1 m, width = 0.1 m and coating thickness = 0.0004 m. The full scale sphere has a diameter = 0.5 m and a coating thickness = 0.002 m. The theoretical sphere has a diameter = 0.1 m and coating

thickness = 0.0004 m. These replicated models were solved using MLFMM and the results from the simulation and the article for the coating plate are shown in Figure 9 (a) – (d), and Figure 10 (a) – (d) for the coating sphere. The FEKO results for both the plate and the sphere lay directly on top of the results from the article with at most 0.05 dBsm difference in some areas.

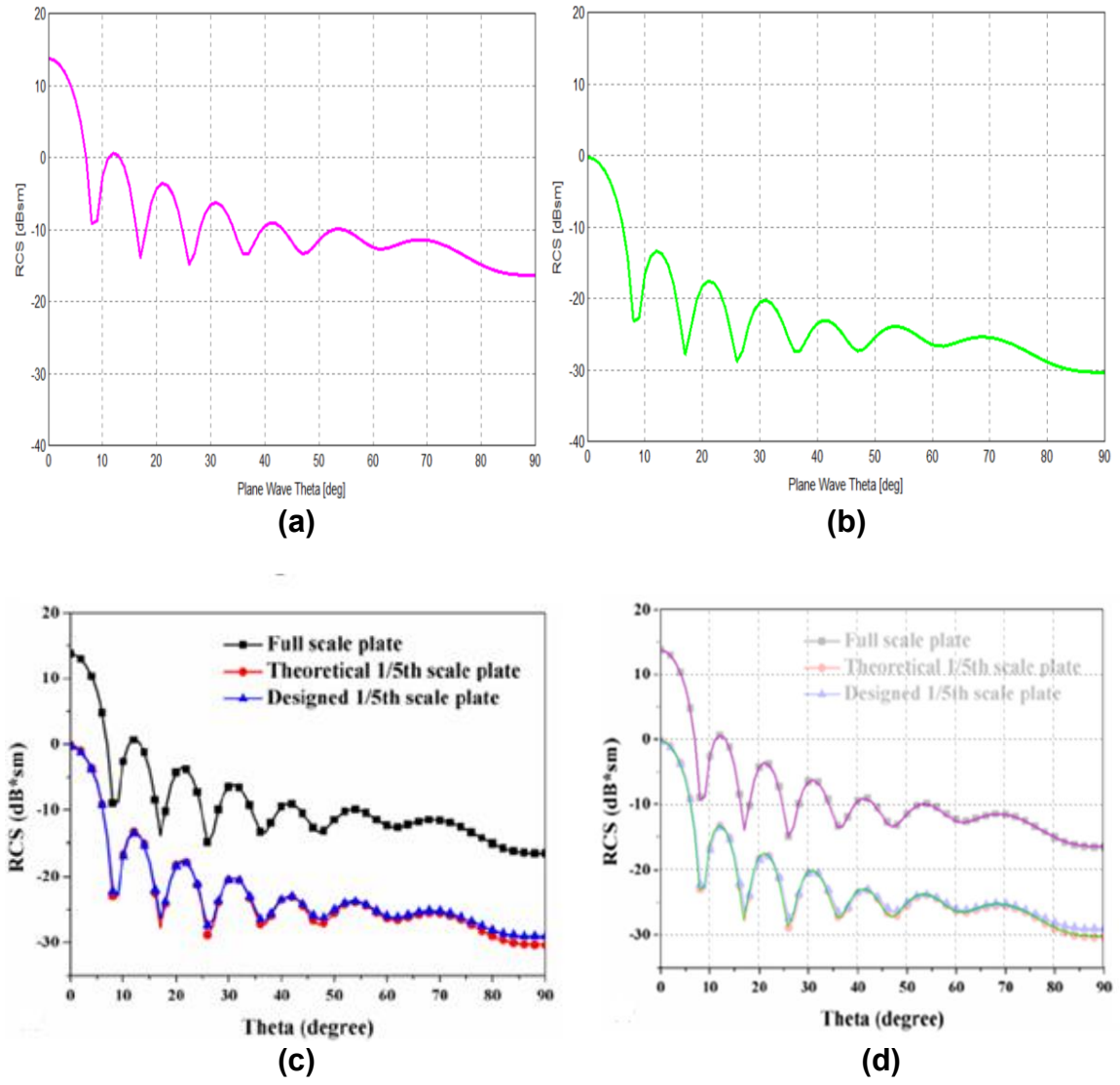

Figure 9: Monostatic HH RCS (dBsm) results from a coating plate: (a) FEKO full scale results, pink line; (b) FEKO theoretical results, green line; (c) article [14] full scale and theoretical results, black line with square (full scale) and red line with circle (theoretical); (d) FEKO results overlaid on the article results.

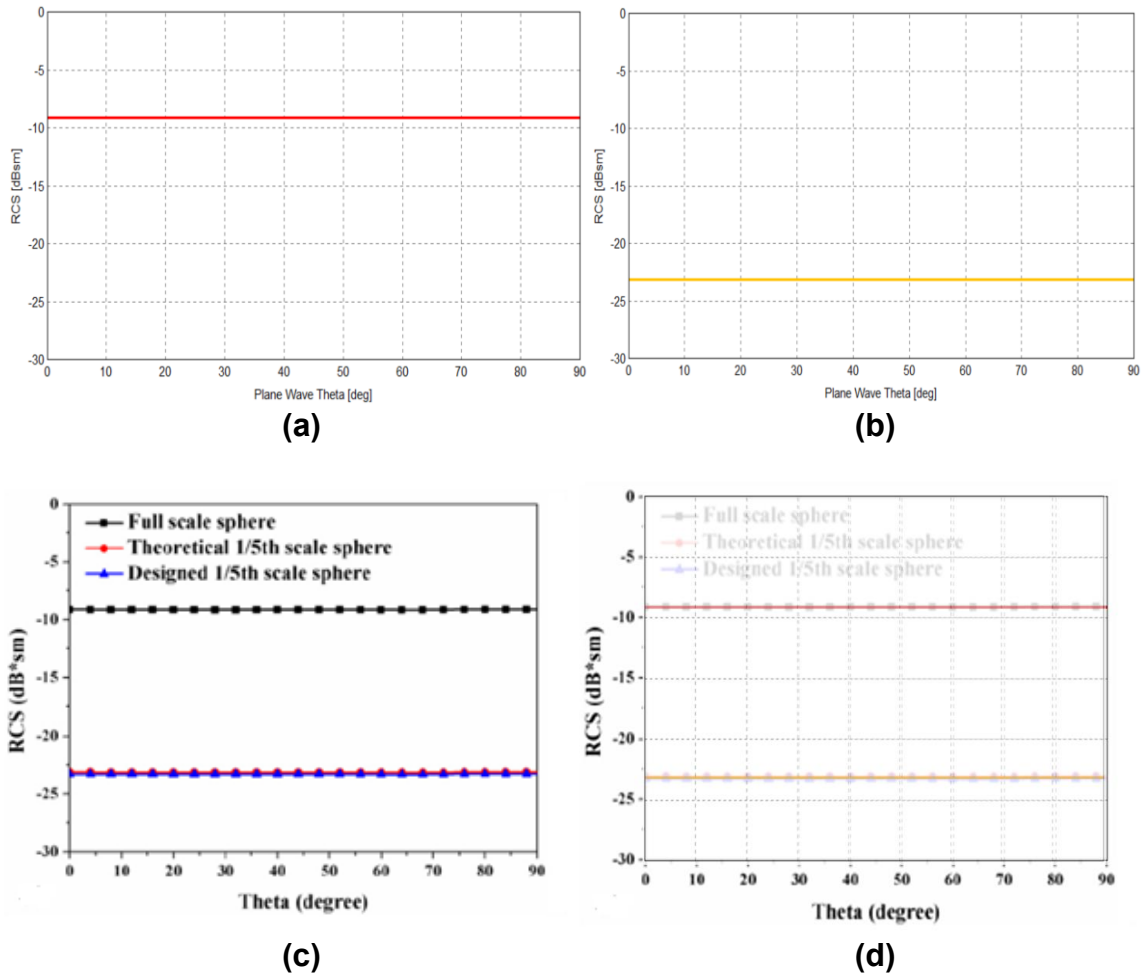

Figure 10: Monostatic HH RCS (dBsm) results from a coating sphere: (a) FEKO full scale results, red line; (b) FEKO theoretical results, orange line; (c) article [14] full scale and theoretical results, black line with square (full scale) and red line with circle (theoretical); (d) FEKO results overlaid on the article results.

3. MODEL VERIFICATION WITH COMPLEX OBJECTS

A more complex model replicated was a PEC triangular trihedral with an extended bottom plate found in [15]. In the report, the methods used are a geometric formula, Xpatch and SAIC full-wave solver (SAF). Xpatch implements the shooting and bouncing ray (SBR) method and SAF implements a MoM and MLFMM hybrid solver. The authors provide results for the geometric formula, the triangular trihedral (VV and HH) and the triangular trihedral with the extended bottom plate (VV and HH). The complex target of interest for model verification is the triangular trihedral with the extended bottom plate. The interior edge dimensions of the triangular trihedral is 0.15 m and the extended bottom plate radius is 0.5 m. The frequency is 10 GHz and the source is an incident plane wave where theta = 75º (elevation = 15º) and phi = 0º - 90º with an increment of 1º. The monostatic RCS is calculated at VV and HH. The asymptotic RL-GO method is used to replicate the results from the report, all of which are seen in Figure 11 (a) – (c). From 20º – 70º the FEKO results align well within 0.25 dBsm of the geometric formula results from the article. The other ranges exhibit characteristics similar to the results in the article but the slight value variations between these results is due to the different solvers that are used.

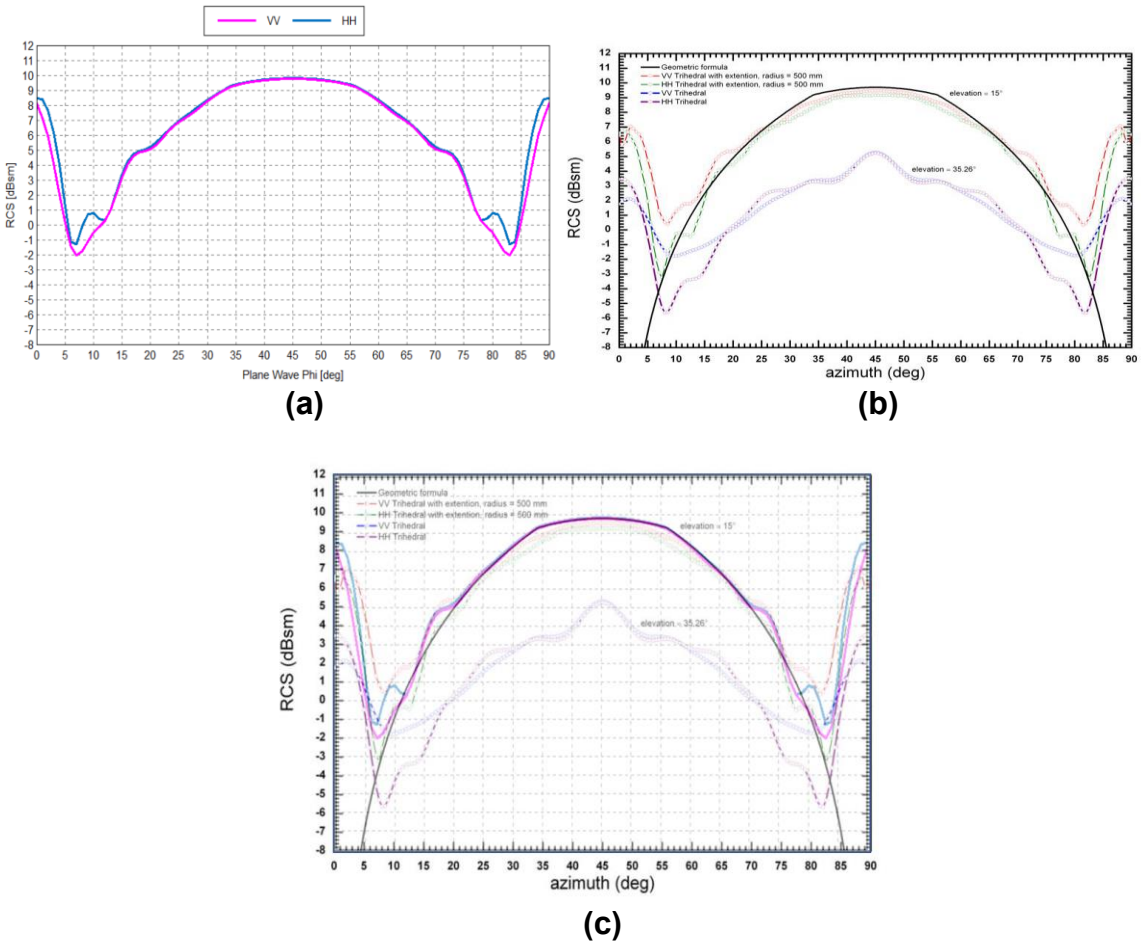

Figure 11: Monostatic VV and HH RCS (dBsm) results from a PEC triangular trihedral with an extended bottom plate: (a) FEKO results, pink line (VV) and blue line (HH); (b) report [15] results, solid black line, red dashed line with circle (VV) and green dashed line with circle (HH); (c) FEKO results overlaid on the report results.

Another complicated object modeled is the real world, well known SAR target, SLICY, (Sandia Laboratories Implementation of Cylinders) that is made up of various reflectors. The CAD model used to replicate results from [16] was provided by [17]. Pictures of both the real target and the CAD model are displayed in Figure 12 (a) & (b). In the article, the results presented are from the proposed scattering center model and the actual RCS data from the SLICY target. For the replicated results in FEKO, RL-GO is used to compute the HH monostatic RCS results with an incident plane wave at theta = 45º and phi = -3.4º to 3.4º with an increment of 0.05º and a frequency of 9 GHz. Figure 13 (a) – (c) show these results versus the results from the article. Characteristics of the FEKO results resemble those provided by the article, however there are some details of the curve that are not matched exactly. This is likely because different SLICY models are used as well as the difference in methods implemented.

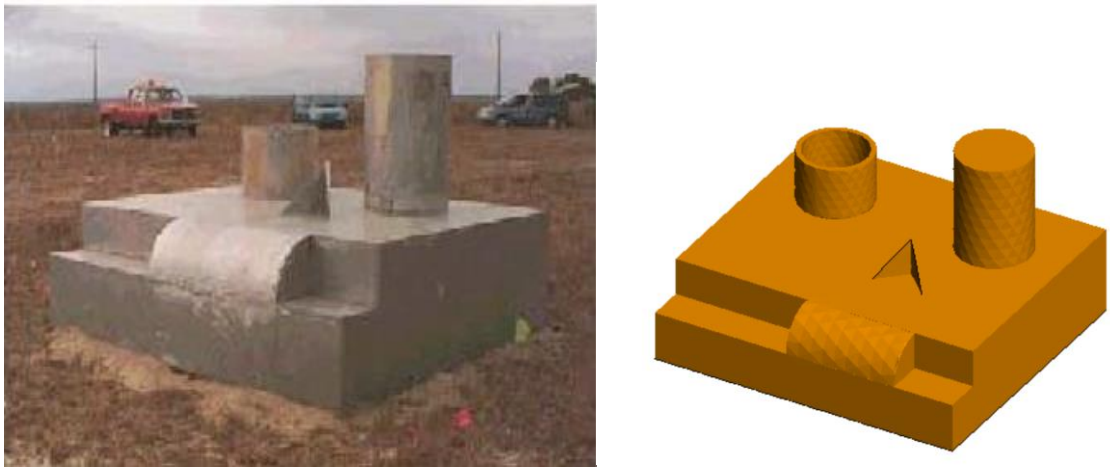

(a) (b)

Figure 12: (a) Photo of the real world SLICY target [18]; (b) Picture of the SLICY CAD model imported into FEKO.

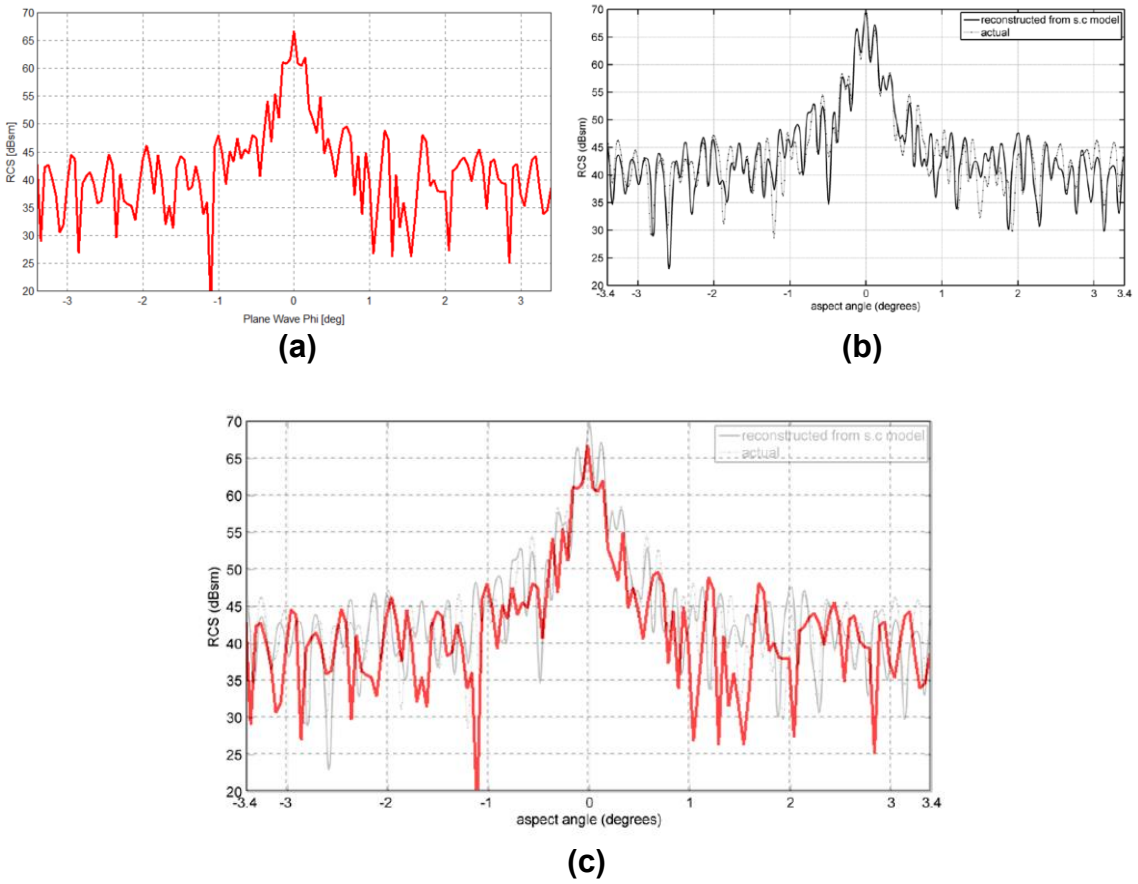

Figure 13: Monostatic HH RCS (dBsm) results from SLICY: (a) FEKO results, red line; (b) article [16] scattering center model results and actual RCS data, solid black line (scattering center model) and black line with a dot (actual RCS data); (c) FEKO results overlaid on the article results.

4. MODEL VALIDATION WITH MEASURED DATA

For a comparison of simulated data versus actual measured data, the monostatic RCS of a 19-inch PEC sphere was measured in one of Sandia National Laboratories (SNL) certified radar testing facilities. The frequency spanned the range 1.85 – 18.25 GHz with the incident plane wave where theta = 0º and phi = 45º. The measured data included the frequency and the RCS magnitude and phase values for both VV and HH. These results were first replicated in FEKO with the PO method because of the large frequency range. The simulated results have a similar curve as the measured data, where the peak to peak oscillations diminish, however, the periodicity is off. This can be seen in Figure 14 (a) – (c) and Figure 15 (a) – (c). To try to resolve this and replicate the measured data more exactly, the MLFMM solver in FEKO was implemented. A smaller frequency range (1.85 – 3 GHz) was selected because of computational restraints using MLFMM, but, the calculation from this subset of frequencies compared even better to the measured data, which is shown in Figure 16 (a) – (c).Thus, using the MLFMM solver captures more signatures and detail of the model.

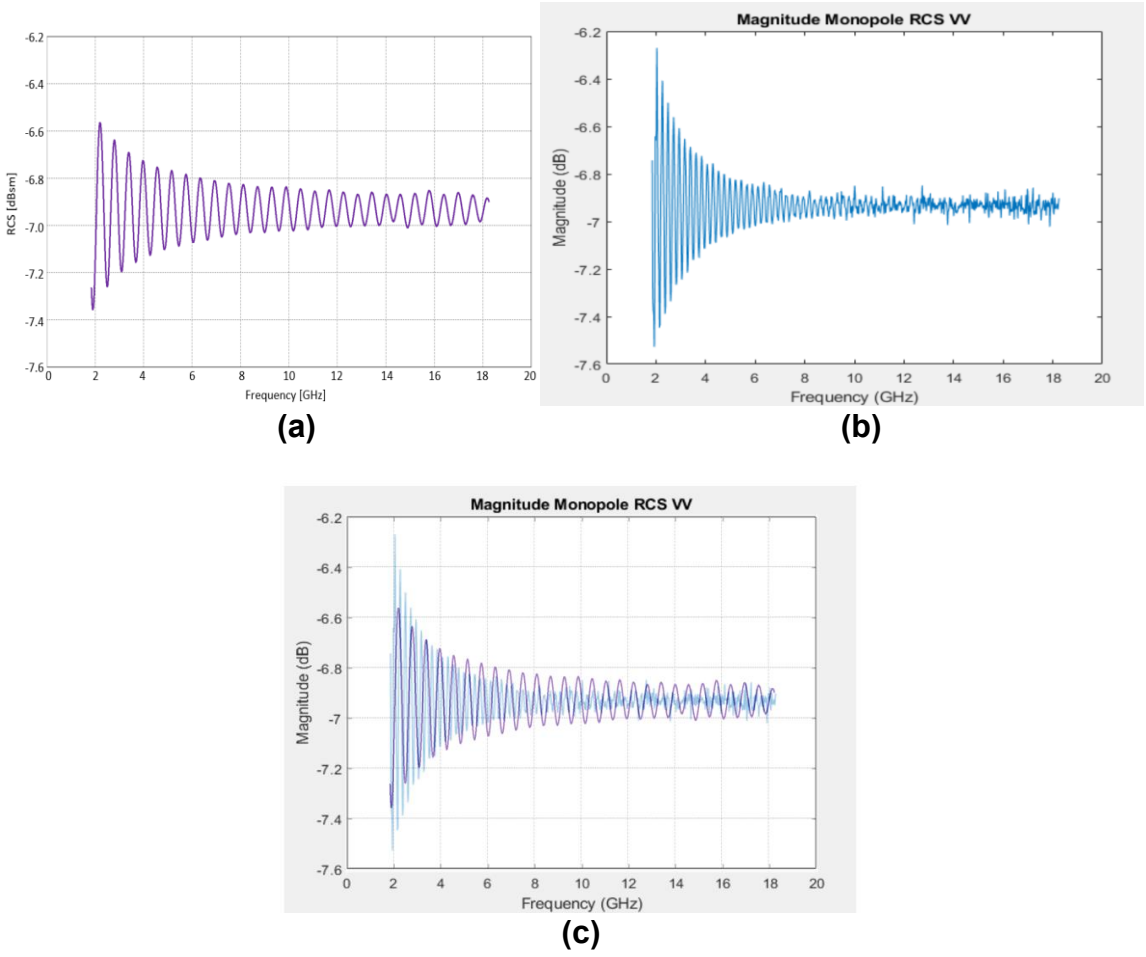

Figure 14: Monostatic VV RCS (dBsm) magnitude results from a 19-inch PEC sphere: (a) FEKO PO results, purple line; (b) measured data, blue line; (c) FEKO results overlaid on the measured data.

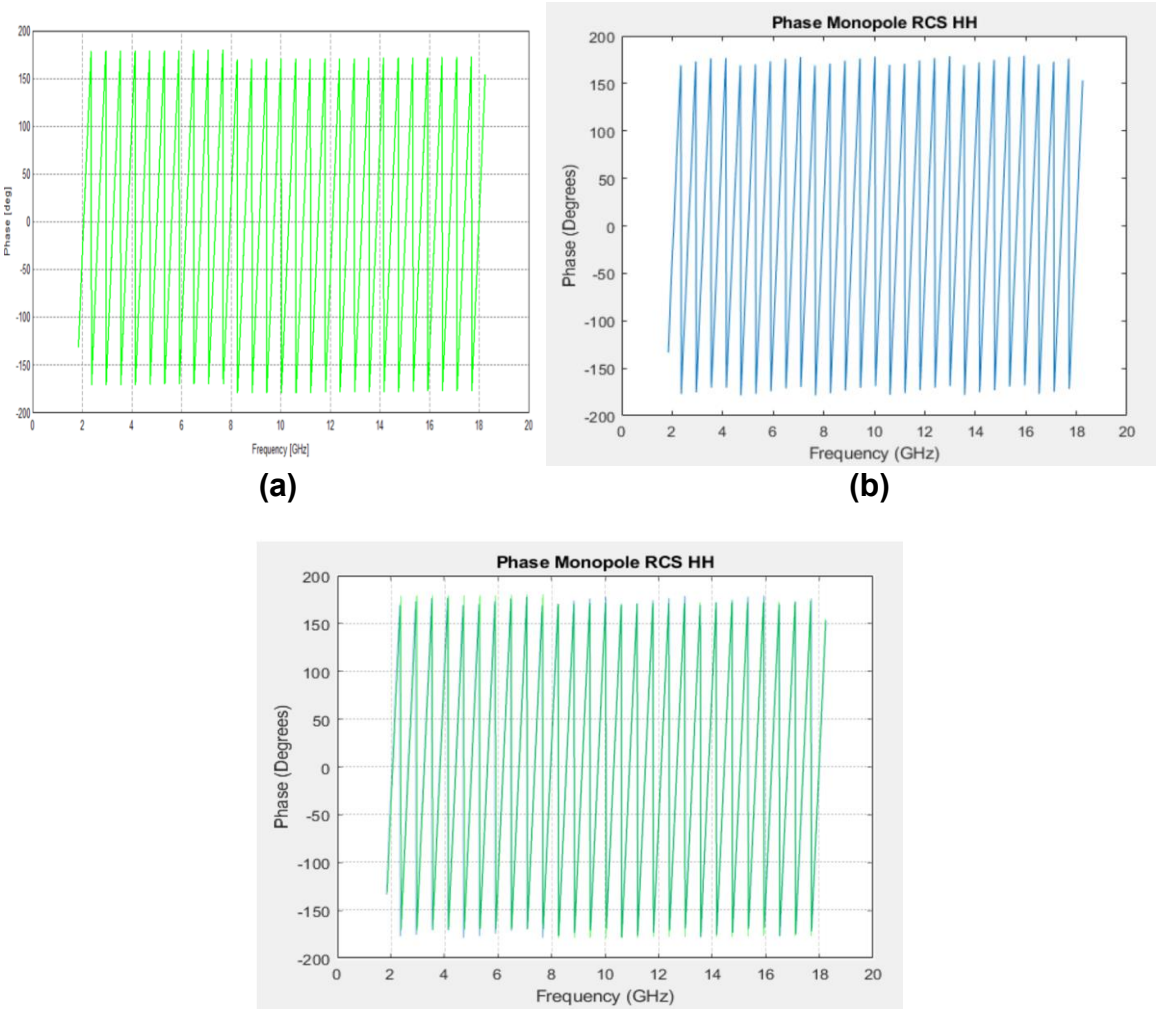

Figure 15: Monostatic HH RCS (dBsm) phase results from a 19-inch PEC sphere: (a) FEKO PO results, green line; (b) measured data, blue line; (c) FEKO results overlaid on the measured data.

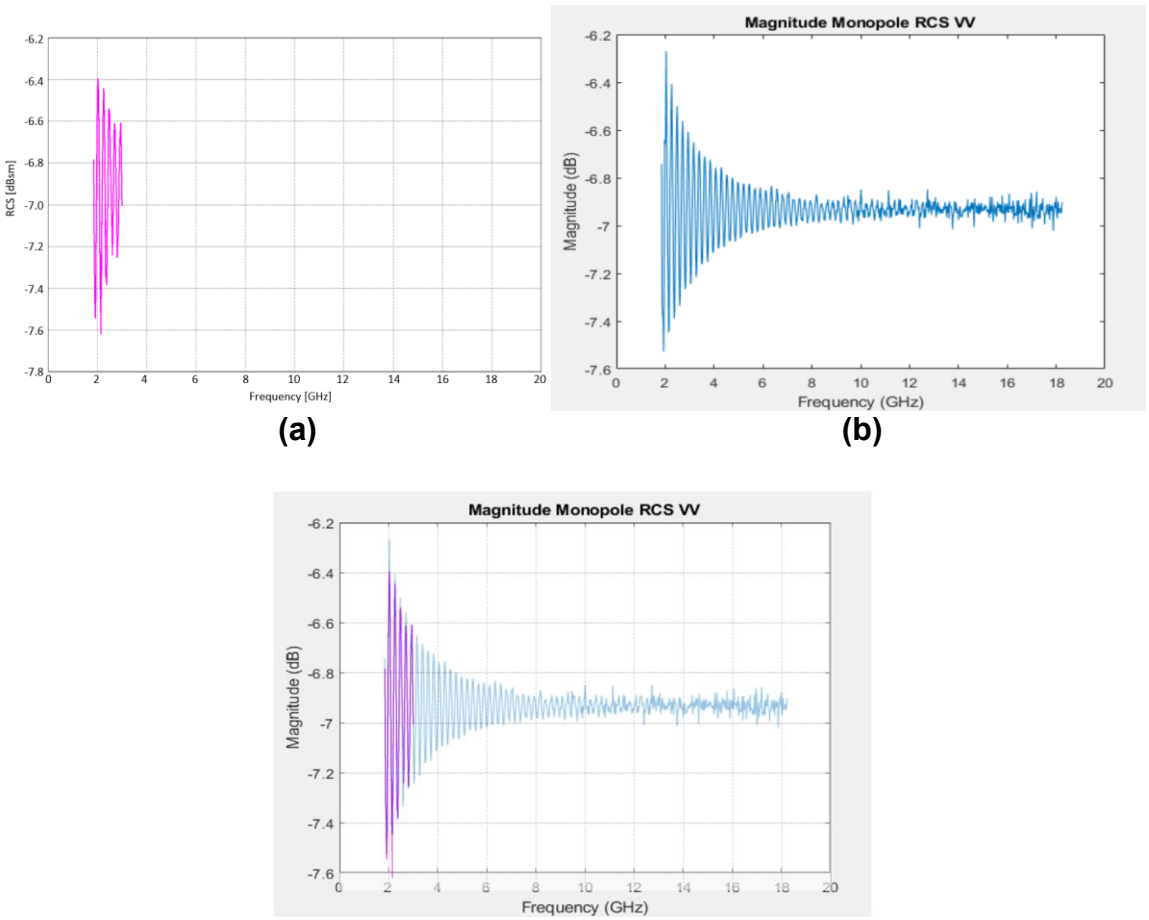

Figure 16: Monostatic VV RCS (dBsm) magnitude results from a 19-inch PEC sphere: (a) FEKO MLFMM results, pink line; (b) measured data, blue line; (c) FEKO MLFMM results overlaid on the measured data.

5. MODEL VERIFICATION WITH A SYMMETRICAL TREE MODEL

Another verification effort involves various simulation scene scenarios using a symmetrical CAD tree model created from scratch in CADFEKO that is described in [4] and [5]. The tree was purposefully designed symmetrically to test for symmetry in order to validate the simulation results. The main purpose of developing this symmetrical tree model was to advance the model verification process to more of a representative model. Each particular scene scenario was chosen to aid with deciphering signals according to EM physics. Thus, while a scenario that uses a ground plane in this section is included, its purpose here is to merely validate the modeling process, and not to explore the effects of the ground on transmissivity properties of the foliage canopy.

The symmetrical tree has trunk, branches and stems created from solid cylinders with varying heights/lengths and diameters. Approximate dimensions of this tree model came from a black walnut tree in [19]. Black walnut trees are deciduous trees, which is a characteristic of interest for this research. The height of the tree is about 4.45 m and the canopy width is around 0.86 m. The trunk diameter is 0.09 m and the thickness of each leaf is 0.0001 m. The MLFMM solver is used because of the size and detail of the tree.

Several different scene scenarios are simulated at 3 different frequencies: L-band (1.25 GHz), X-band (9.6 GHz) and Ku-band (15 GHz). The model scenarios are: (1) a symmetrical dielectric tree in free space, (2) a symmetrical PEC tree in free space (3) a symmetrical dielectric tree on a soil ground plane and (4) 2 symmetrical dielectric trees located 2 m apart in free space (simulated only at L-band). The ground plane is a built in FEKO homogenous half space in region $Z < 0$, which is a reflection coefficient approximation. This ground plane is assigned a dielectric value of soil with a dielectric constant of $\varepsilon_r = 5.0 - j0.7$ for all frequencies, which is referenced in [19]. Most of the tree properties and frequencies come from [19]. The dielectric values of the leaves and the trunk of the symmetrical tree model are calculated by the dielectric value model equation discussed in [4] and [5] and derived and detailed in [20]. All the calculated dielectric values assume a temperature of 22 ºC, bulk density of 0.33 and a gravimetric moisture content of 0.68. At L-band (1.25 GHz), the relative permittivity of the leaves is $\varepsilon_r = 28.0383 - j9.0076$ and the relative permittivity of the trunk and branches is $\varepsilon_r = 28.4047 - j9.0651$. The X-band (9.6 GHz) and Ku-band (15 GHz) trunk and branch materials have to be modeled with an impedance sheet because MLFMM cannot handle high loss material. At X-band the relative permittivity of the leaves is $\varepsilon_r = 20.75 - j8.8838$ and the trunk and branches relative permittivity is $\varepsilon_r = 21.092 - j9.0229$ with a surface impedance of $Z_s = 20.0432 + j18.0831$. For Ku-band, the relative permittivity of the leaves is $\varepsilon_r = 17.4081 - j9.5048$ and the trunk/branches/stems relative permittivity is $\varepsilon_r = 17.6857 + j9.6739$ with a surface impedance of $Z_s = 21.3453 + j19.2526$.

Two different incident plane waves are simulated at theta = -50º, phi = 0º and theta = 50º, phi = 0º for all the scenarios at each frequency. The choice of incident angle for FOPEN radar operation involved trading the line-of-sight path-length through the canopy against the image distortions inherent to steep collection geometries. Generally,

an incident angle in the vicinity of 45º is considered a good operational compromise. The bistatic RCS is recorded for theta = -90º to 90º; increment of 5º, and phi = 0º with a polarization of VV. Figure 17 displays the symmetrical tree with the simulation parameters in FEKO.

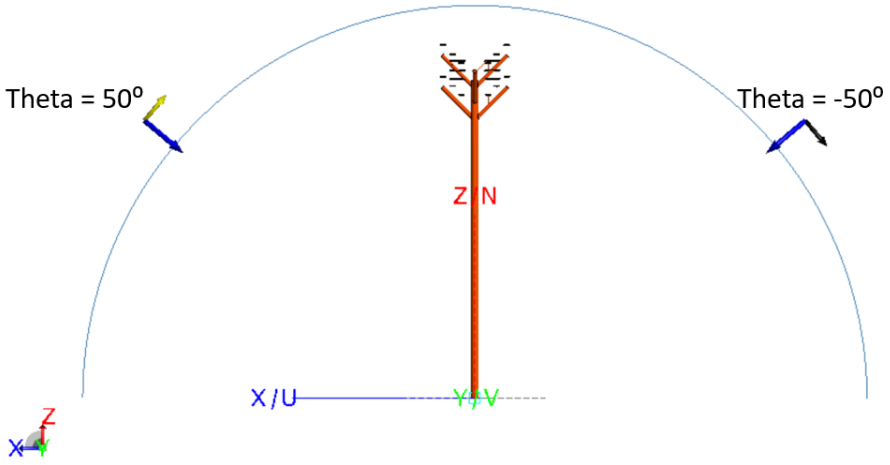

Figure 17: Symmetrical tree and simulation setup in FEKO with an incident angle of theta = -50º, phi = 90º and theta = 50º, phi = 90º.

The bistatic RCS results with plane wave theta = -50º and theta = 50º are symmetrical for all scenarios at each frequency. The mirrored RCS results are indistinguishable, and this demonstrates that the setup and the solver are outputting expected results. For L-band, these results are viewed in Figure 18 (a) - (c) for a symmetrical dielectric tree in free space, Figure 19 (a) - (c) for a symmetrical PEC tree in free space, Figure 20 (a) - (c) for a symmetrical dielectric tree over a soil ground plane and Figure 21 (a) - (c) for two symmetrical dielectric trees located 2 m apart in free space. For X-band, the results are displayed in Figure 22 (a) - (c) for a symmetrical dielectric tree in free space, Figure 23 (a) - (c) for a symmetrical PEC tree in free space and Figure 24 (a) - (c) for a symmetrical dielectric tree over a soil ground plane. For Ku-band the results are shown in Figure 25 (a) - (c) for a symmetrical dielectric tree in free space, Figure 26 (a) - (c) for a symmetrical PEC tree in free space and Figure 27 (a) - (c) for a symmetrical dielectric tree over a soil ground plane.

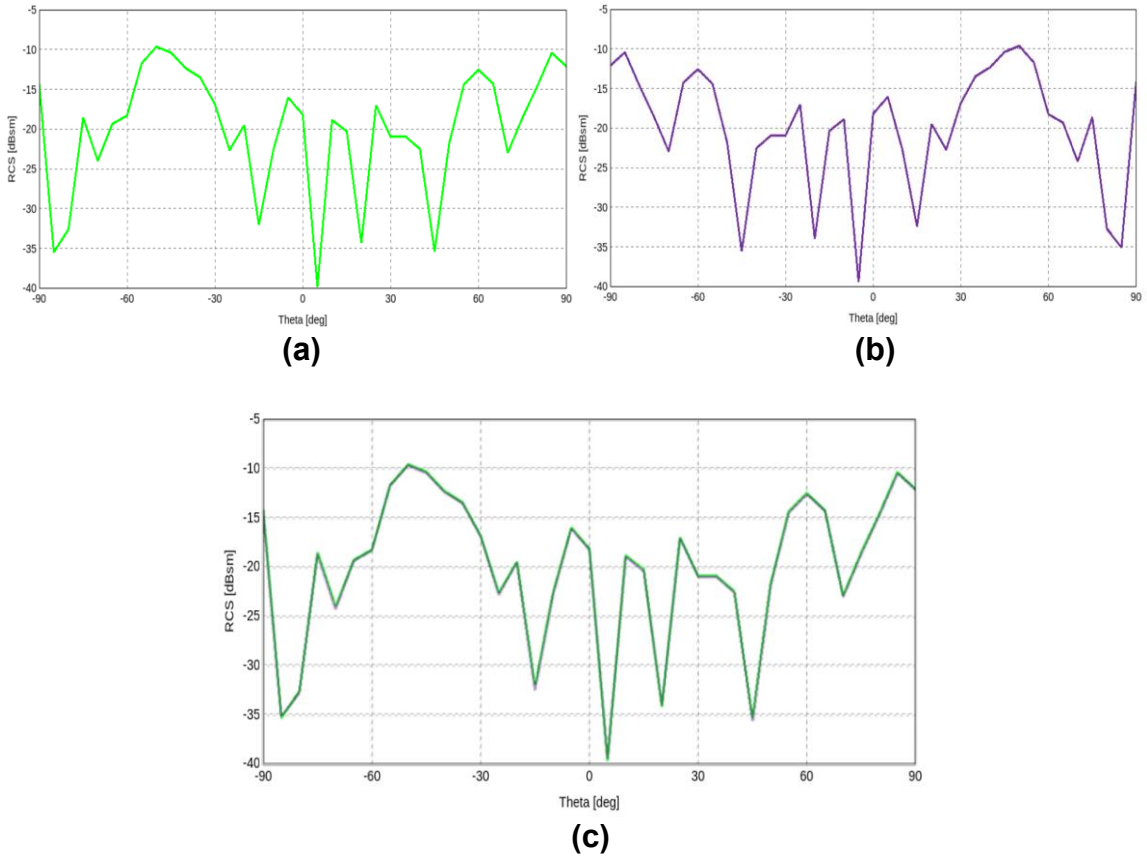

Figure 18: Bistatic VV RCS (dBsm) results for a symmetrical dielectric tree in free space at L-band for: (a) incident plane wave theta = -50º; (b) incident plane wave theta = 50º; (c) incident plane wave theta = 50º (purple line) reversed and overlaid on incident plane wave theta = -50º (green line).

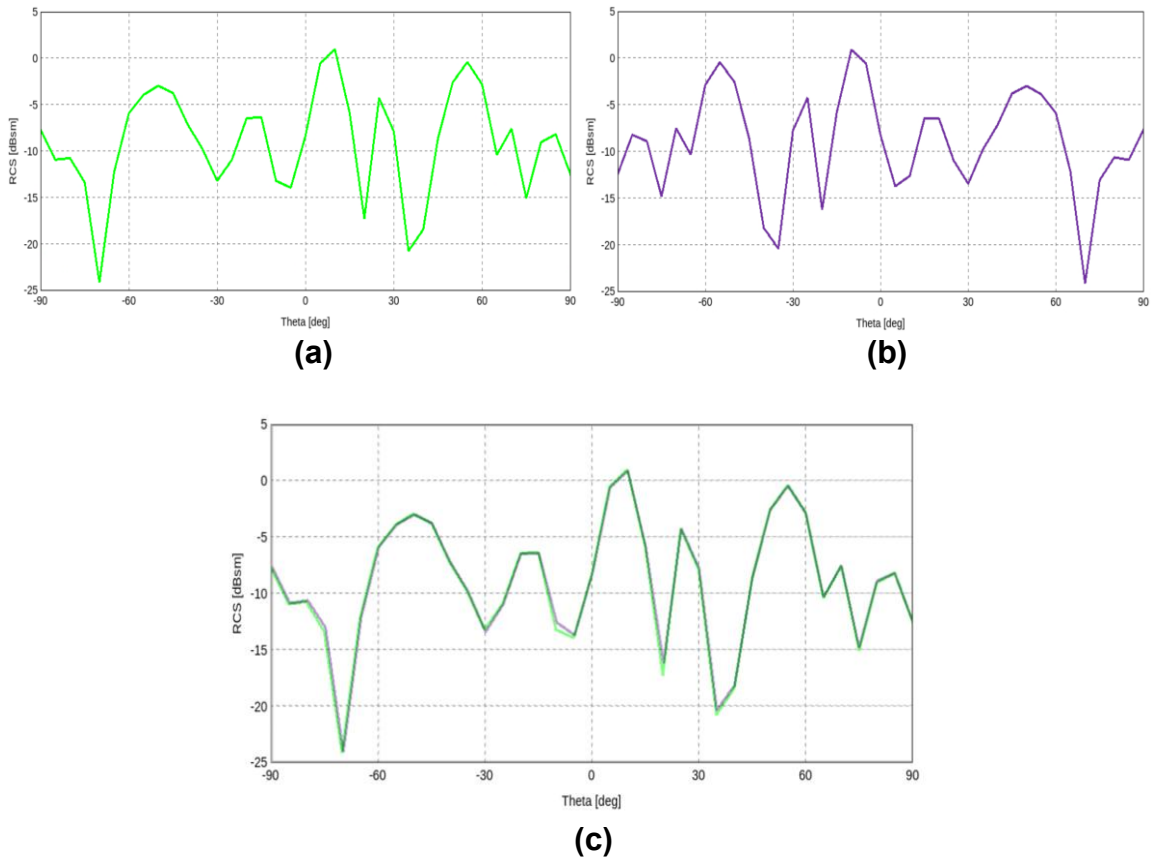

Figure 19: Bistatic VV RCS (dBsm) results for a symmetrical PEC tree in free space at L-band for: (a) incident plane wave theta = -50º; (b) incident plane wave theta = 50º; (c) incident plane wave theta = 50º (purple line) reversed and overlaid on incident plane wave theta = -50º (green line).

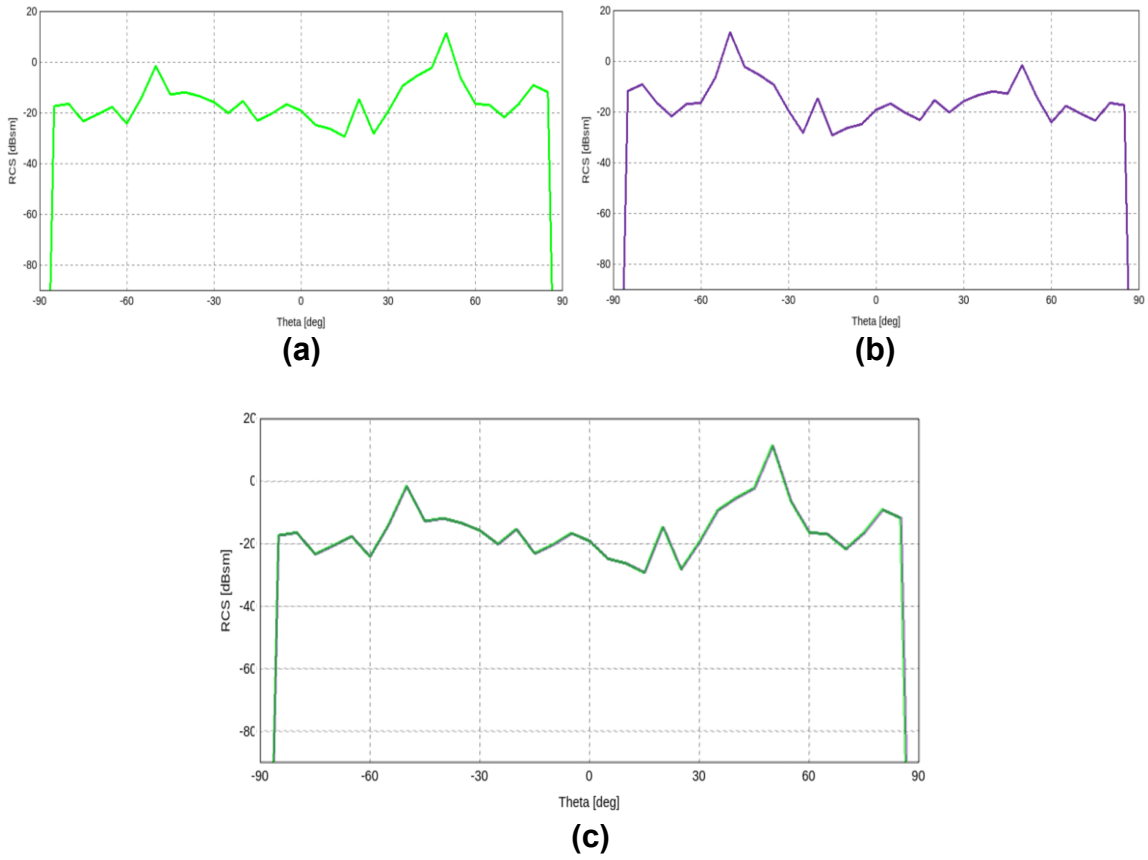

Figure 20: Bistatic VV RCS (dBsm) results for a symmetrical dielectric tree over a soil ground plane at L-band for: (a) incident plane wave theta = -50º; (b) incident plane wave theta = 50º; (c) incident plane wave theta = 50º (purple line) reversed and overlaid on incident plane wave theta = -50º (green line).

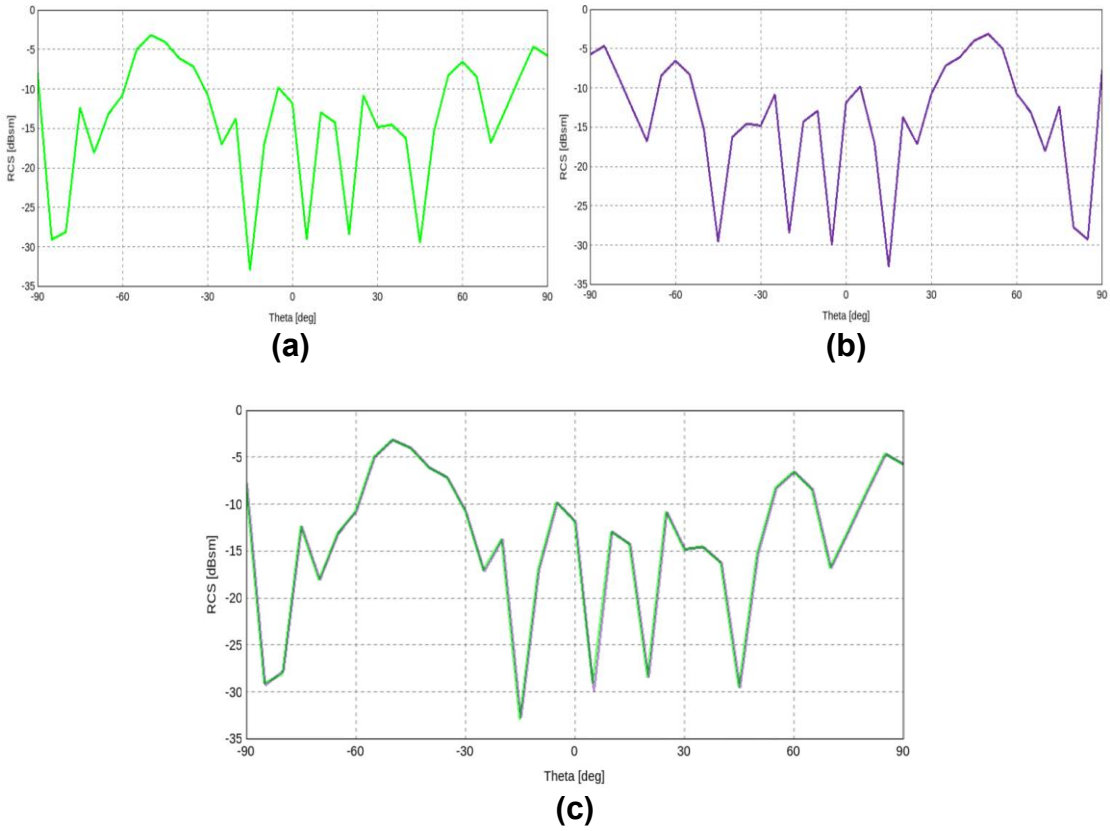

Figure 21: Bistatic VV RCS (dBsm) results for 2 symmetrical dielectric trees located 2 m apart in free space at L-band for: (a) incident plane wave theta = -50º; (b) incident plane wave theta = 50º; (c) incident plane wave theta = 50º (purple line) reversed and overlaid on incident plane wave theta = -50º (green line).

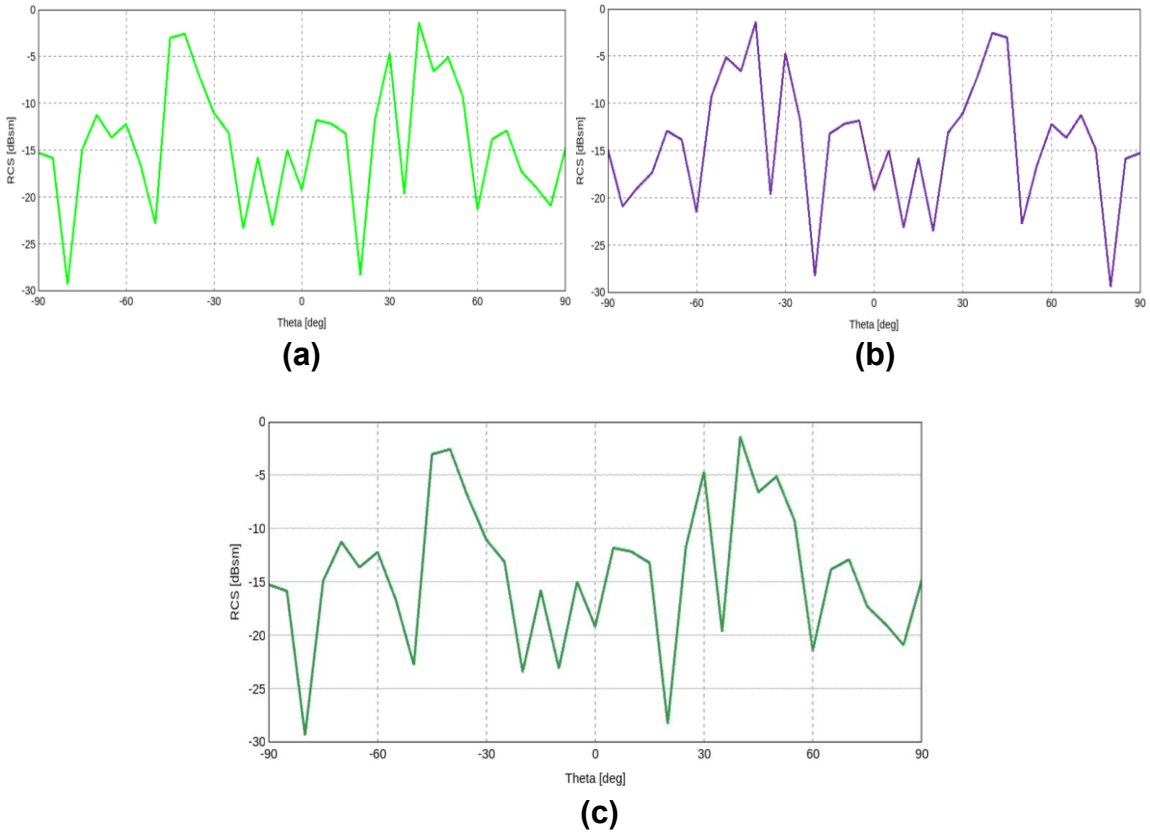

Figure 22: Bistatic VV RCS (dBsm) results for a symmetrical dielectric tree in free space at X-band for: (a) incident plane wave theta = -50º; (b) incident plane wave theta = 50º; (c) incident plane wave theta = 50º (purple line) reversed and overlaid on incident plane wave theta = -50º (green line).

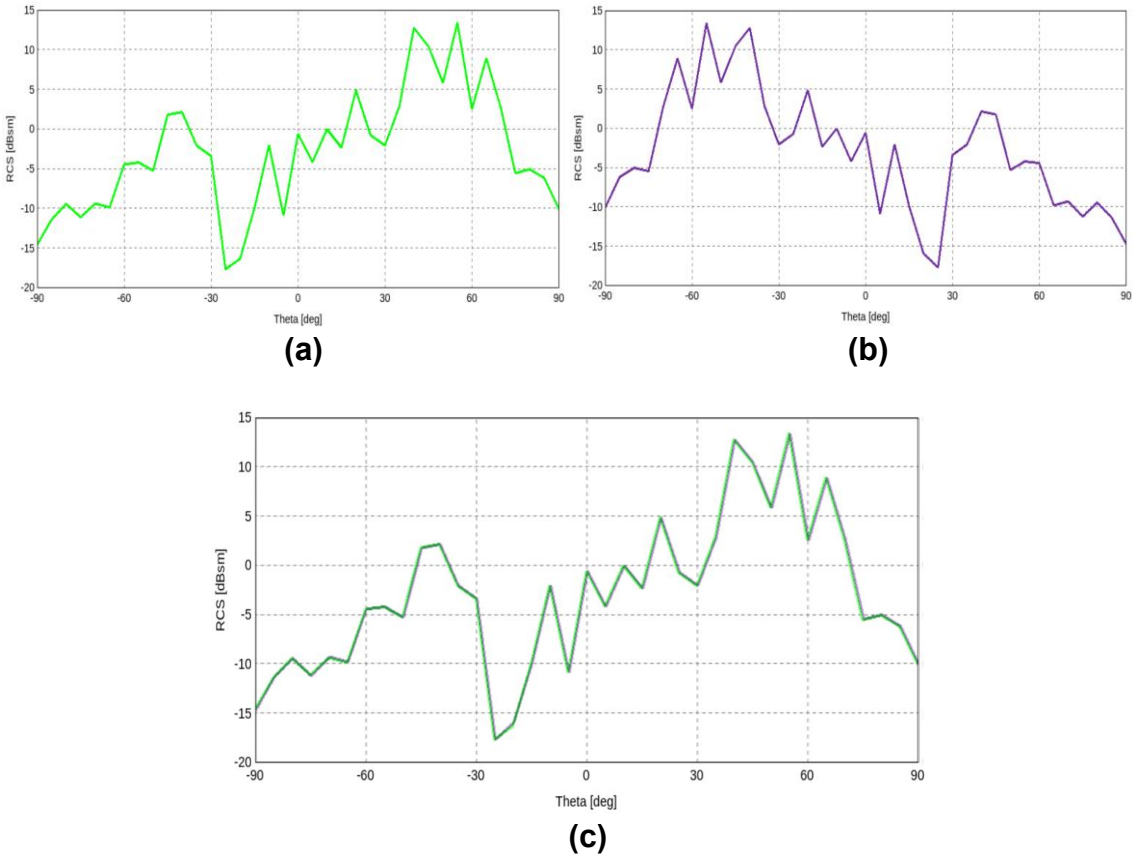

Figure 23: Bistatic VV RCS (dBsm) results for a symmetrical PEC tree in free space at X-band for: (a) incident plane wave theta = -50º; (b) incident plane wave theta = 50º; (c) incident plane wave theta = 50º (purple line) reversed and overlaid on incident plane wave theta = -50º (green line).

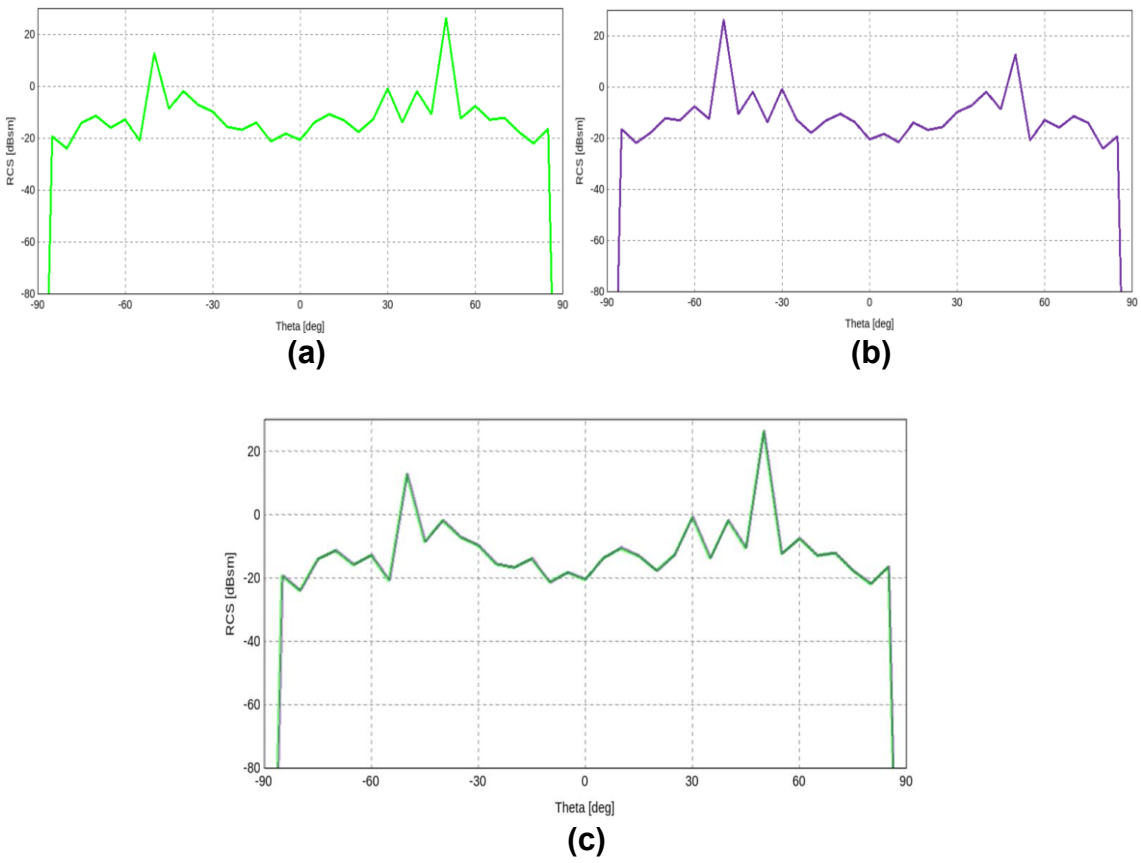

Figure 24: Bistatic VV RCS (dBsm) results for a symmetrical dielectric tree over a soil ground plane at X-band for: (a) incident plane wave theta = -50º; (b) incident plane wave theta = 50º; (c) incident plane wave theta = 50º (purple line) reversed and overlaid on incident plane wave theta = -50º (green line).

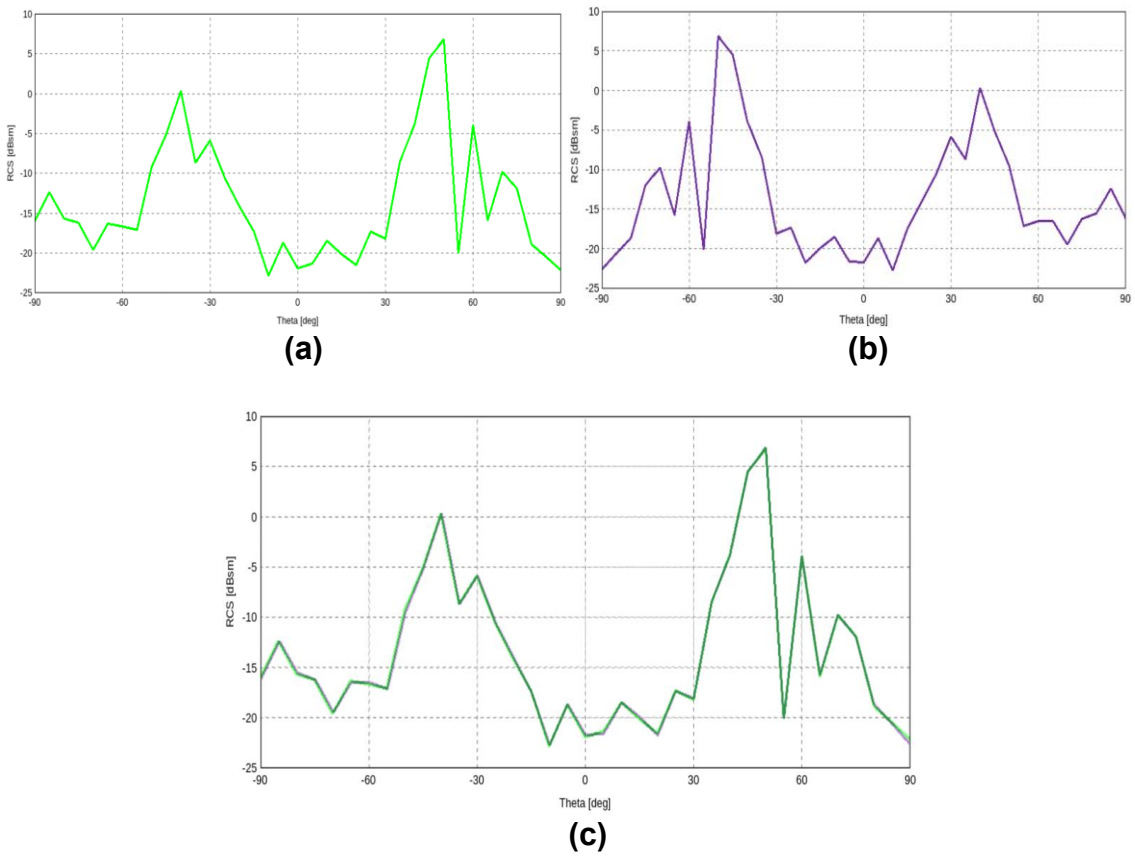

Figure 25: Bistatic VV RCS (dBsm) results for a symmetrical dielectric tree in free space at Ku-band for: (a) incident plane wave theta = -50º; (b) incident plane wave theta = 50º; (c) incident plane wave theta = 50º (purple line) reversed and overlaid on incident plane wave theta = -50º (green line).

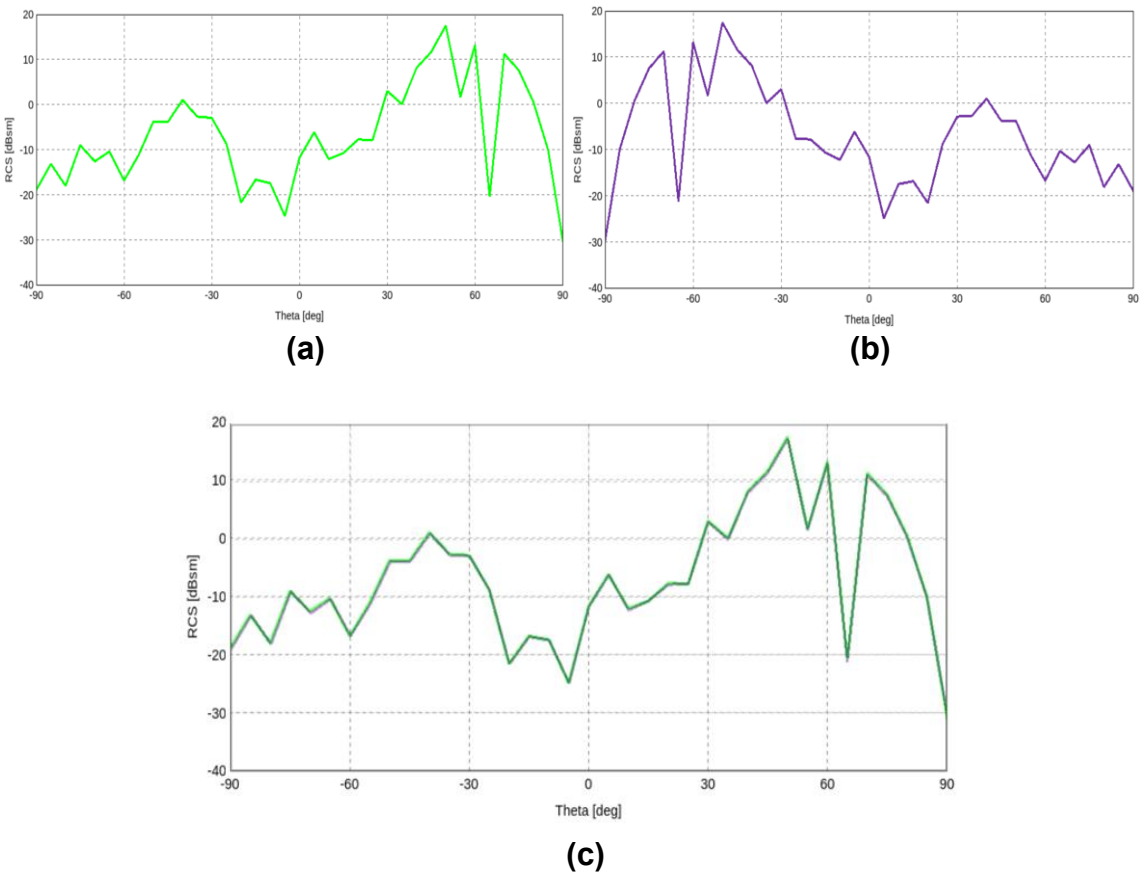

Figure 26: Bistatic VV RCS (dBsm) results for a symmetrical PEC tree in free space at Ku-band for: (a) incident plane wave theta = -50º; (b) incident plane wave theta = 50º; (c) incident plane wave theta = 50º (purple line) reversed and overlaid on incident plane wave theta = -50º (green line).

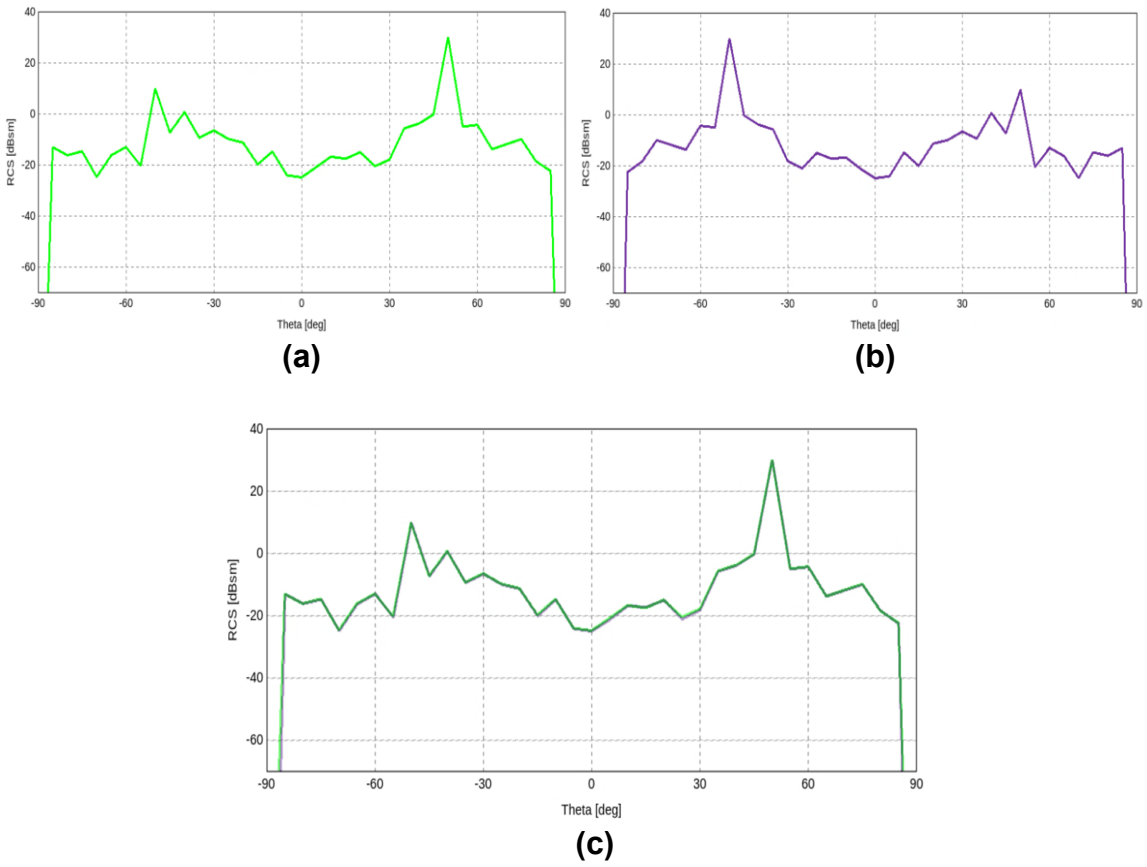

Figure 27: Bistatic VV RCS (dBsm) results for a symmetrical dielectric tree over a soil ground plane at Ku-band for: (a) incident plane wave theta = -50º; (b) incident plane wave theta = 50º; (c) incident plane wave theta = 50º (purple line) reversed and overlaid on incident plane wave theta = -50º (green line).

When comparing every scene setup at one frequency, the interest is to assess the trends and see if the RCS results comply with the physics of EM, and this is the case. There is more reflection from the PEC tree in free space than the dielectric tree in free space, and the dielectric tree over a ground plane has the highest RCS values compared to the other scenarios. For example, at L-band, the average RCS for the dielectric tree in free space is around -23 dBsm, for the PEC tree in free space the average RCS is around -12 dBsm, the dielectric tree over a ground plane is about -5 dBsm and the two dielectric trees in free space is approximately -17 dBsm. A comparison of every scenario for each frequency with an incident plane wave theta = 50º are displayed in Figure 28 (a) – (d) for L-band, Figure 29 (a) – (c) for X-band and Figure 30 (a) – (c) for Ku-band.

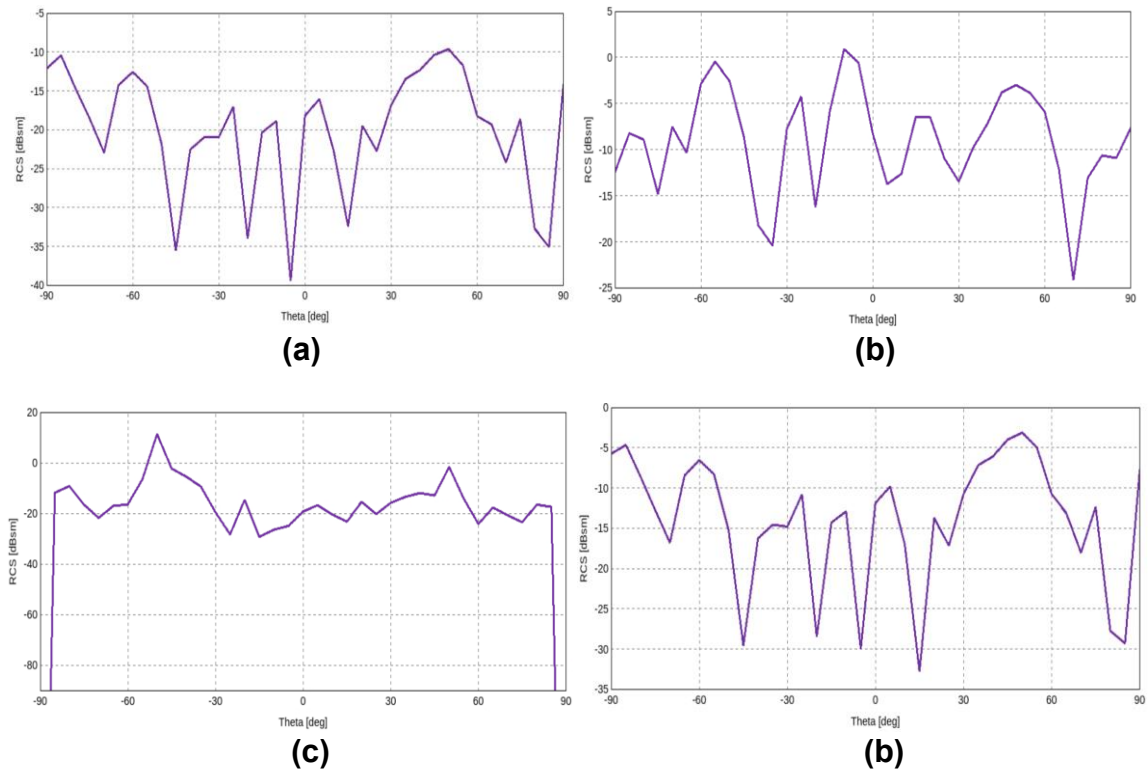

Figure 28: Bistatic VV RCS (dBsm) results at L-band for incident plane wave theta = 50º: (a) a symmetrical dielectric tree in free space; (b) a symmetrical PEC tree in free space; (c) a symmetrical dielectric tree on a soil ground plane; and (d) 2 symmetrical dielectric trees located 2 m apart in free space.

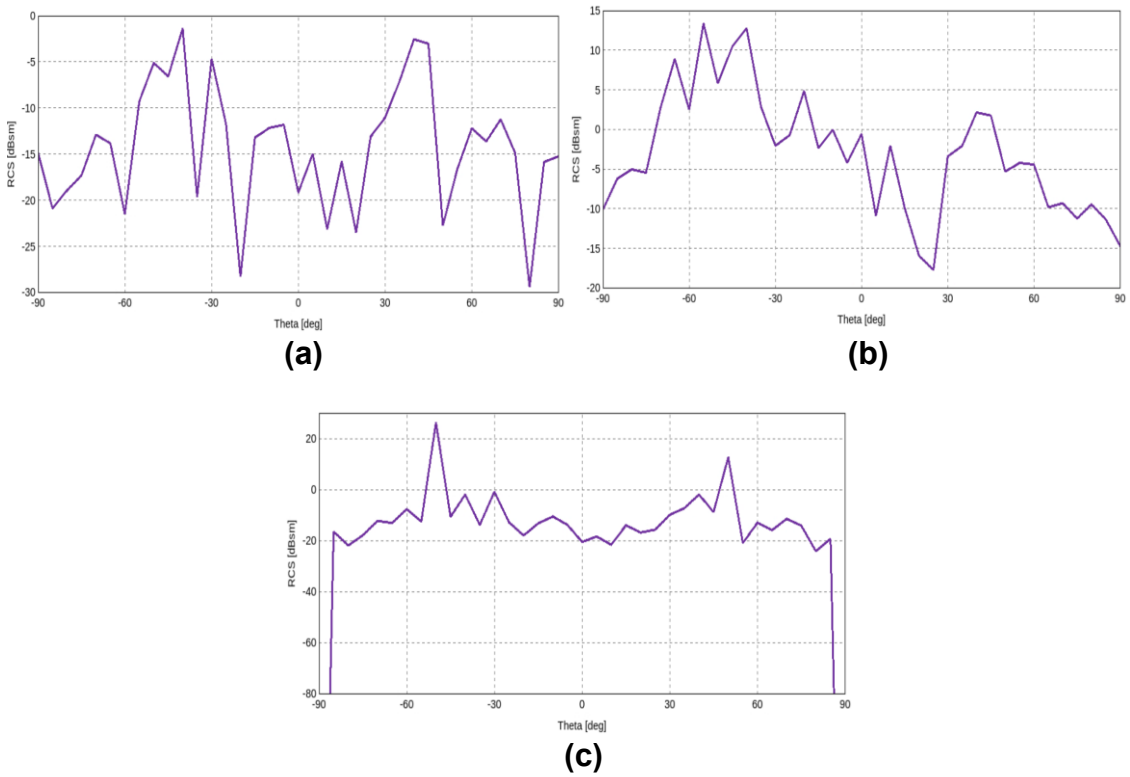

Figure 29: Bistatic VV RCS (dBsm) results at X-band for incident plane wave theta = 50º: (a) a symmetrical dielectric tree in free space; (b) a symmetrical PEC tree in free space; (c) a symmetrical dielectric tree on a soil ground plane.

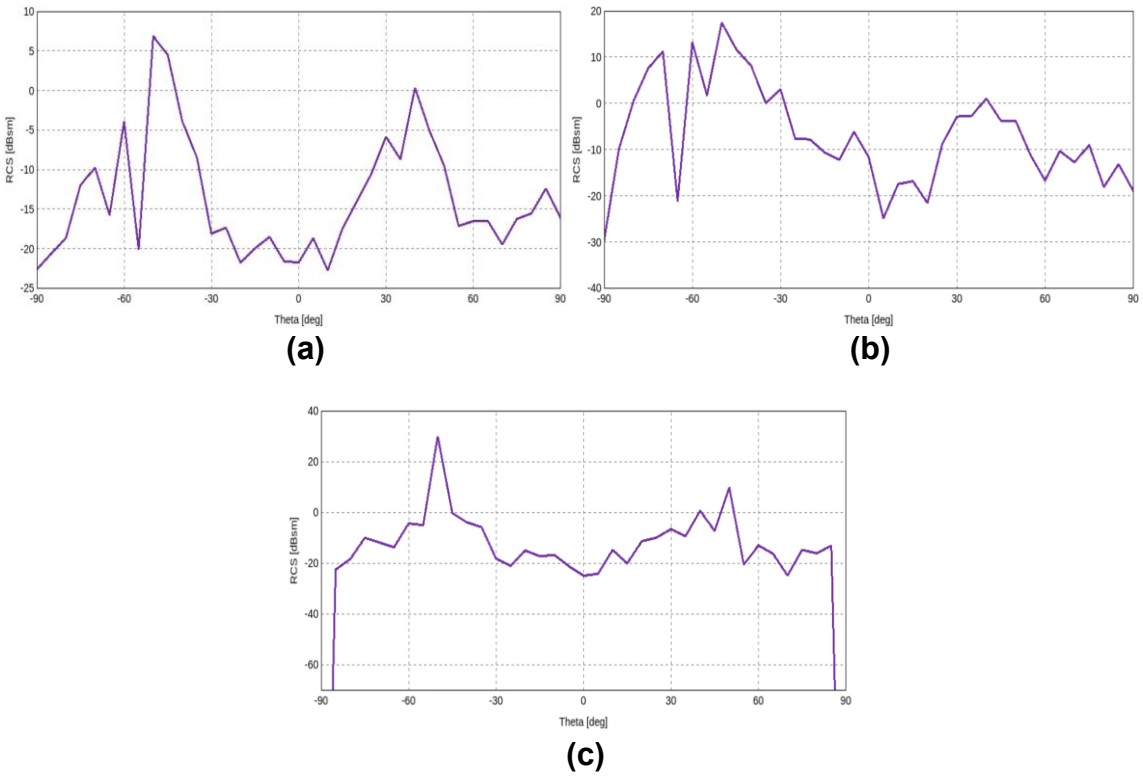

Figure 30: Bistatic VV RCS (dBsm) results at Ku-band for incident plane wave theta = 50º: (a) a symmetrical dielectric tree in free space; (b) a symmetrical PEC tree in free space; (c) a symmetrical dielectric tree on a soil ground plane.

In addition, each scenario was compared across the three frequencies. These results make sense as well with L-band having lower RCS values (i.e. less scattering) and Ku-band having the highest RCS values (i.e. the most scattering). For instance, the scene with a dielectric tree over a soil ground plan has an average RCS of -20 dBsm for L-band, -18 dBsm for X-band and -10 dBsm for Ku-band. These frequency comparison graphs are shown in Figure 31 (a) – (c) for a symmetrical dielectric tree in free space, Figure 32 (a) – (c) for a symmetrical PEC tree in free space, and Figure 33 (a) – (c) for a symmetrical dielectric tree on a soil ground plane. All the results verify that the solver and the solver setup are implemented and simulating correctly.

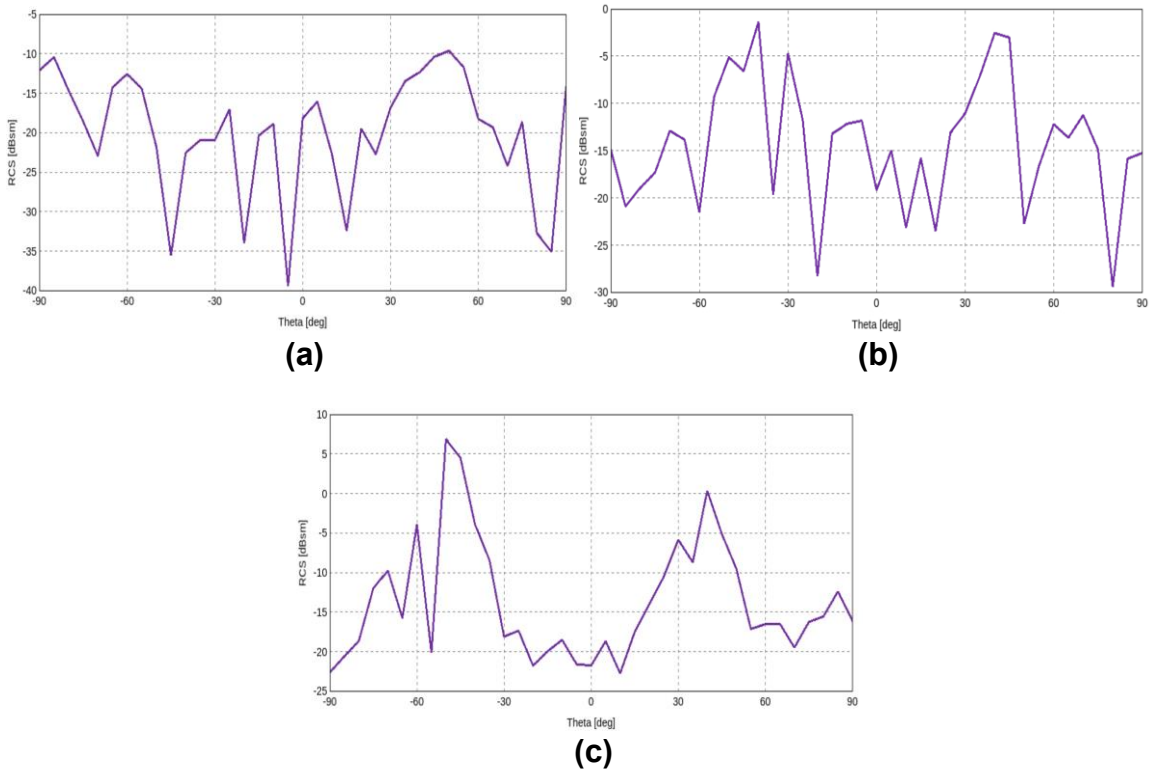

Figure 31: Bistatic VV RCS (dBsm) results for a symmetrical dielectric tree in free space with incident plane wave theta = 50º: (a) L-band; (b) X-band; (c) Ku-band.

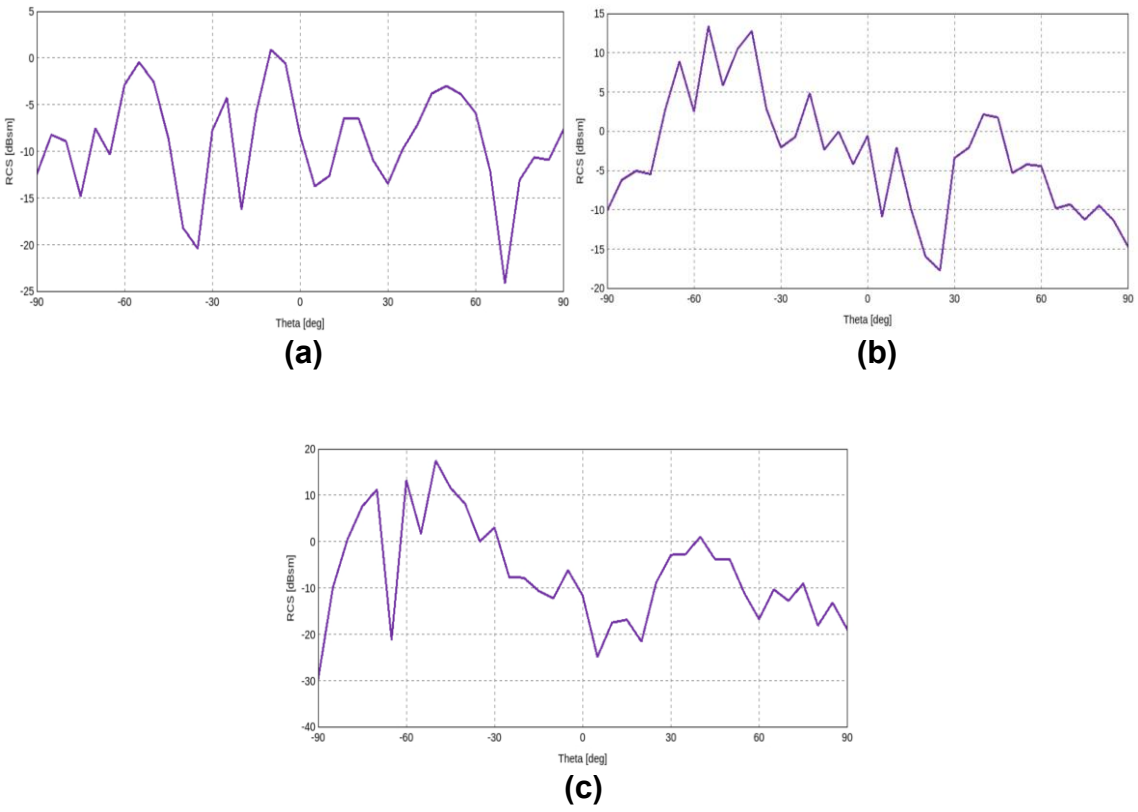

Figure 32: Bistatic VV RCS (dBsm) results for a symmetrical PEC tree in free space with incident plane wave theta = 50º: (a) L-band; (b) X-band; (c) Ku-band.

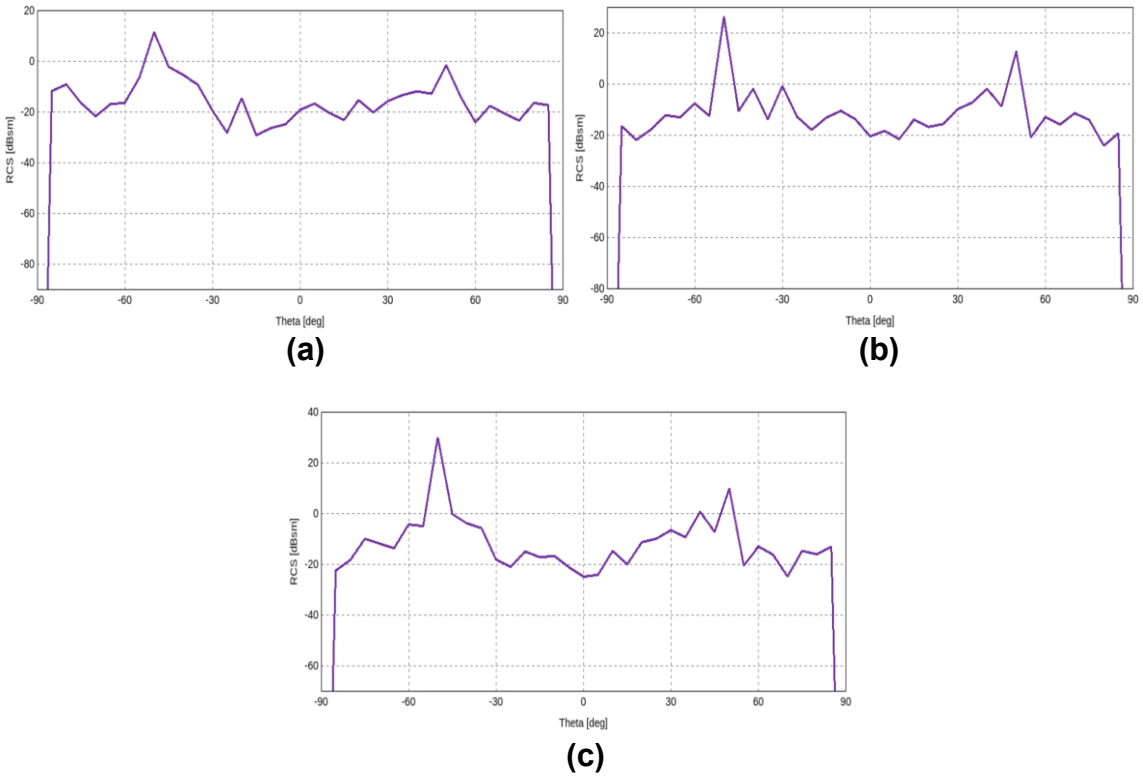

Figure 33: Bistatic VV RCS (dBsm) results for a symmetrical dielectric tree on a soil ground plane with incident plane wave theta = 50º: (a) L-band; (b) X-band; (c) Ku-band.

Additional verification simulations were carried out where the dielectric tree model in free space was solved without leaves (trunk and branches only) and with leaves (full tree) at each frequency. These results also proved to confirm the integrity of the solver and the model. At L-band, there was a negligible difference in the results between the tree with leaves and the tree without leaves. The average RCS for both cases is around -23 dBsm. This was expected since the wavelengths at this frequency (0.24 m) are very large compared to the leaves and thus do not significantly contribute to the scattering. The average RCS results at X-band for the tree model without leaves is around -17 dBsm and for the tree model with leaves the average RCS is around -14 dBsm. At Ku-band the results for the tree model without leaves average around -15 and the average RCS value for the tree model with leaves is approximately -12 dBsm. Thus, the tree models with leaves at X-band, and even more so at Ku-band, have an increased scattering effect since as the frequency increases the wavelengths gets smaller and the size of the leaves become larger relative to the smaller wavelengths, consequently creating more scattering. These RCS value comparisons are presented in Figure 34 (a) & (b) for L-band, Figure 35 (a) & (b) for X-band and Figure 36 (a) & (b) for Ku-band.

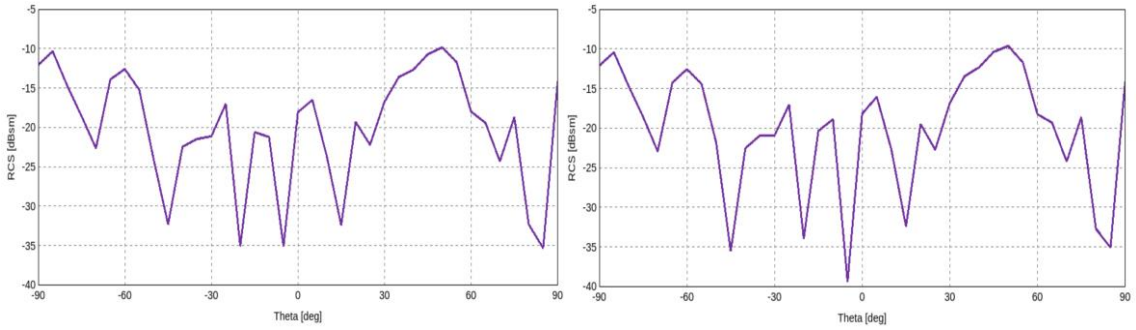

Figure 34: Bistatic VV RCS (dBsm) results for a symmetrical dielectric tree in free space with incident plane wave theta = 50º at L-band: (a) without leaves (trunk and branches only) and (b) with leaves (full tree).

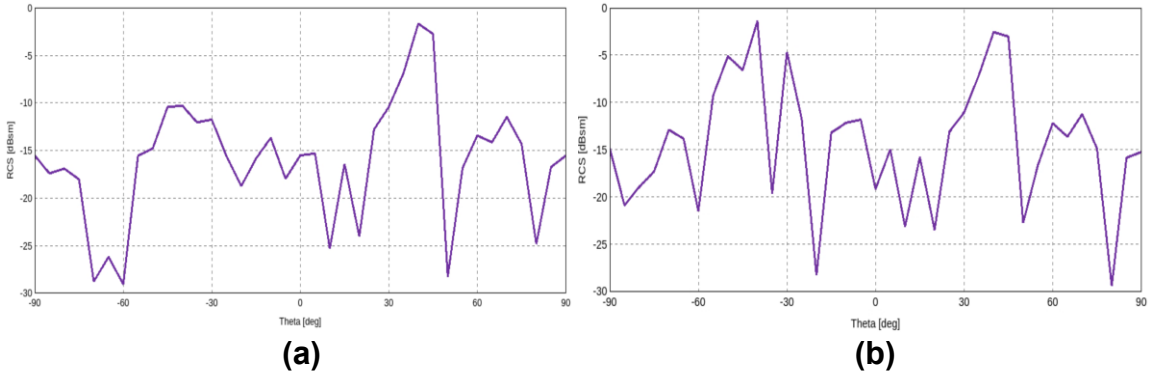

Figure 35: Bistatic VV RCS (dBsm) results for a symmetrical dielectric tree in free space with incident plane wave theta = 50º at X-band: (a) without leaves (trunk and branches only) and (b) with leaves (full tree).

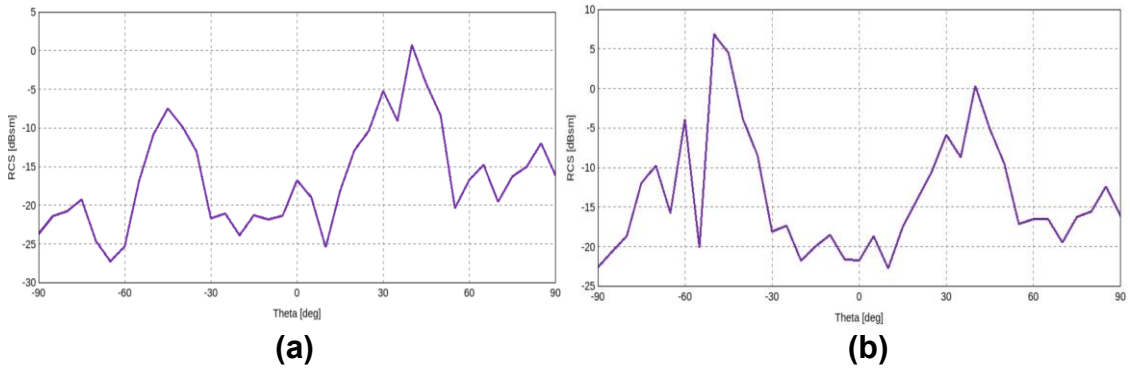

Figure 36: Bistatic VV RCS (dBsm) results for a symmetrical dielectric tree in free space with incident plane wave theta = 50º at Ku-band: (a) without leaves (trunk and branches only) and (b) with leaves (full tree).

6. MODEL VERIFICATION WITH A CAD TREE MODEL

For further verification, a CAD tree model created in Arbaro was implemented to simulate results from an article where an Arbaro CAD tree model was also employed [21]. The authors used the quaking aspen CAD tree file from the Arbaro library to analyze scattering characterizations. They used the FDTD method to solve the problem at low frequencies from 200 – 500 MHz (P-band). Since the contribution from the leaves on the tree is negligible at these low frequencies, simulations in this article were carried out for the tree trunk only, the tree trunk with primary branches and the tree trunk with primary and secondary branches (Figure 37). The tree height is 7.4 m and the base diameter is 0.34 m. The trunk has a relative permittivity of 13.9 and a conductivity of 0.039 S/m. The ground plane is soil with a relative permittivity of 5.45 and a conductivity of 0.020 S/m. The monostatic RCS results with polarizations VV and HH are calculated with an incident plane wave of theta = 45º, 60º, 75º and an averaging of the responses over 36 phi angles. For the replicated results in FEKO, MLFMM was used to simulate the trunk only model over a soil ground plane of homogenous half space in region Z < 0 (reflection coefficient approximation) (Figure 37). The trunk model imported into FEKO was created from the quaking aspen Arbaro CAD tree library file. Because an averaging of phi angles cannot directly be calculated in FEKO, different selected phi angles were calculated and compared with the phi averaging results calculated in the article, which are displayed in Figure 38 (a) – (d) for an incident angle of theta = 45º, phi = 45º, 90º and 225º; Figure 39 (a) & (b) for incident angle theta = 60º, phi = 45º; and Figure 40 (a) & (b) for incident angle theta = 75º, phi = 45º.

The results in the article and the replicated results are similar. The curves follow the same trend and are within comparable dB ranges, however, they are not exact. This can be due to the variation of how the phi angle is handled. Also, the article does not explain how the ground plane was solved so this could be the difference as well. In addition, not having the exact tree model or tree model orientation will give at least a slight variance in results. Lastly, calculating the RCS with different solvers can cause varying plots.

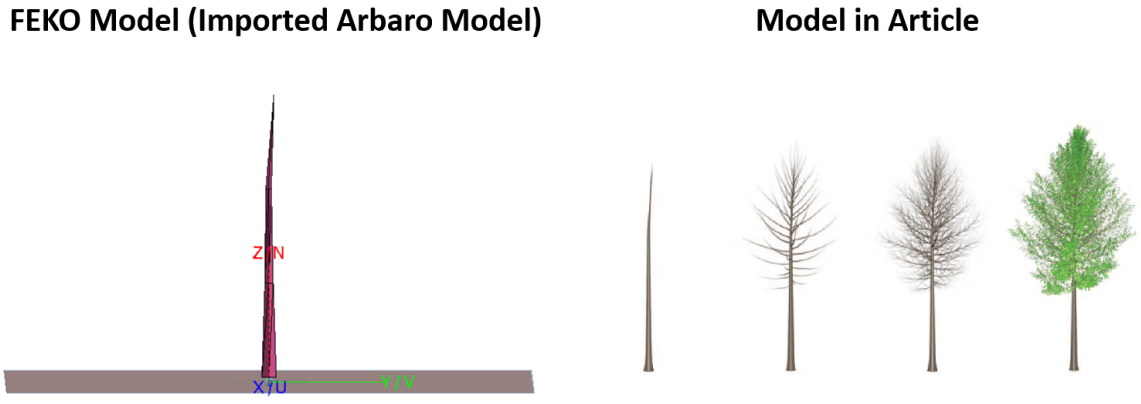

Figure 37: Side by side comparison of the imported quaking aspen trunk only tree model in FEKO and the various models of the tree in the article [21].

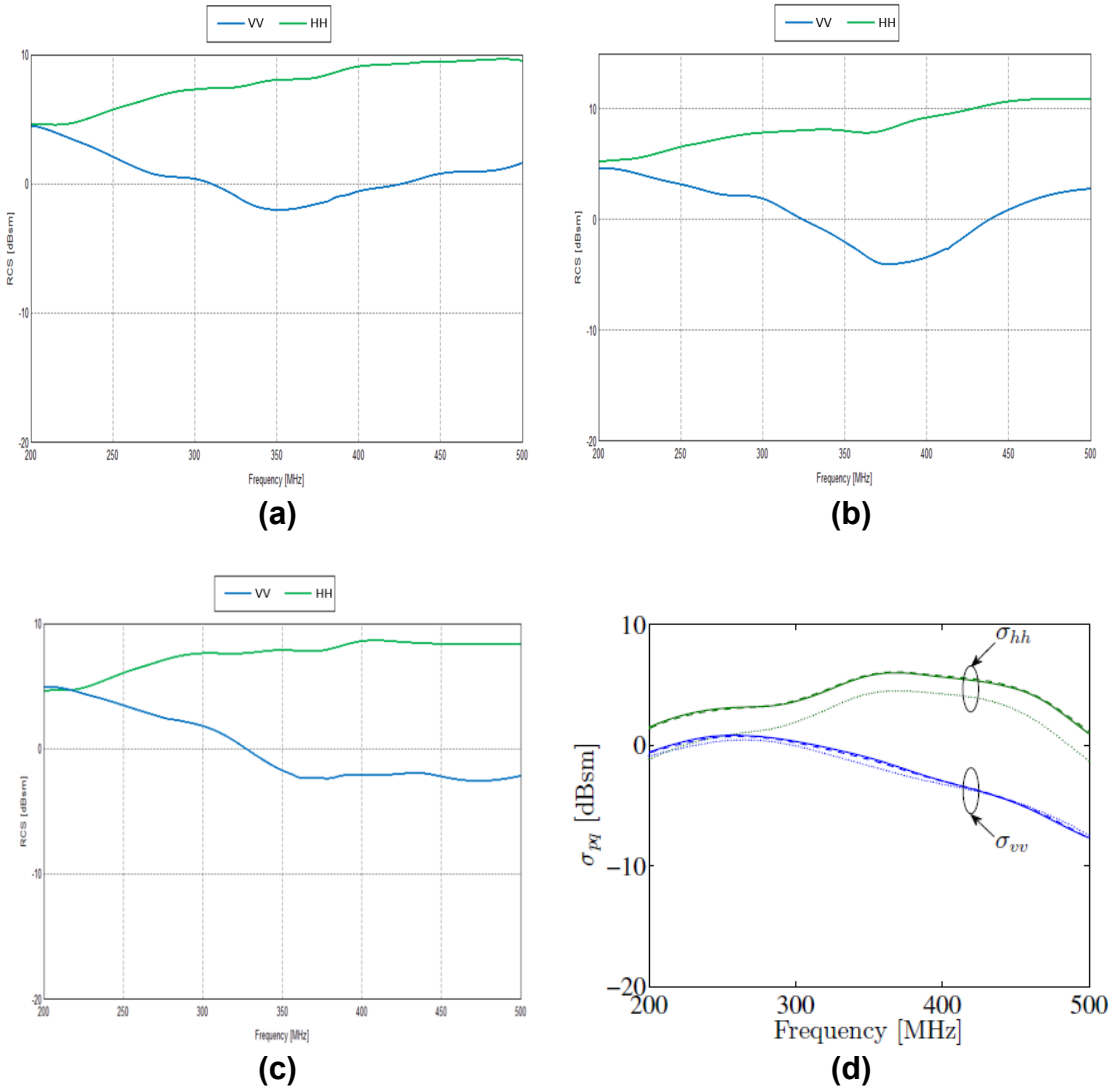

Figure 38: Monostatic VV (blue lines) and HH (green lines) RCS (dBsm) results from a quaking aspen tree trunk: (a) FEKO results for theta = 45º, phi = 45º; (b) FEKO results for theta = 45º, phi = 90º; (c) FEKO results for theta = 45º, phi = 225º; (d) article results [21] for theta = 45º, an average of 36 phi angles; dotted lines (trunk), dashed lines (trunk and primary branches), solid lines (trunk, primary and secondary branches).

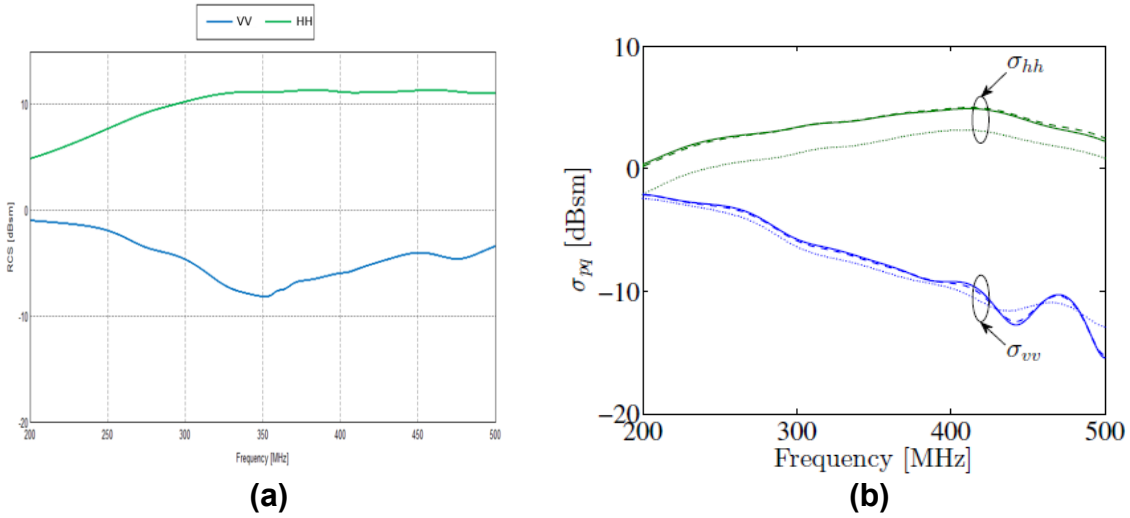

Figure 39: Monostatic VV (blue lines) and HH (green lines) RCS (dBsm) from a quaking aspen tree trunk: (a) FEKO results for theta = 60º, phi = 45º and (b) article [21] results for theta = 60º, an average of 36 phi angles; dotted lines (trunk), dashed lines (trunk and primary branches), solid lines (trunk, primary and secondary branches).

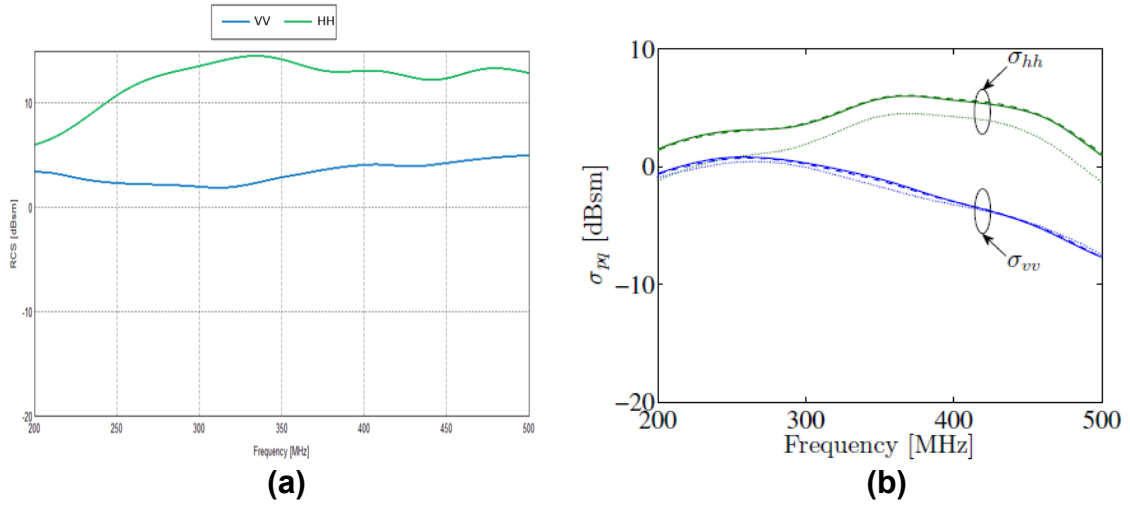

Figure 40: Monostatic VV (blue line) and HH (green line) RCS (dBsm) from a quaking aspen tree trunk: (a) FEKO results for theta = 75º, phi = 45º and (b) article [21] results for theta = 75º, an average of 36 phi angles; dotted lines (trunk), dashed lines (trunk and primary branches), solid lines (trunk, primary and secondary branches).

7. CONCLUSION

Several diverse model simulations were replicated for verification and validation of the CEM software and the accuracy of setup. Different methods were utilized for familiarity with each one and as a preliminary exercise to find the appropriate and optimal solver for the FOPEN research problem. Verification started with simple canonical models from articles then advanced to more complex models. For a more complete validation process, measured data was replicated, and eventually the verification process progressed to a full symmetrical tree model and an externally designed imported CAD tree trunk model.

Through these exploratory simulations and being advised by Altair FEKO engineers, MLFMM is deemed the optimal method to solve simulations of an EM wave interactions with realistic full tree models at higher frequencies. This is because MLFMM is best suited for solving electrically large problems (large trees at high frequencies) with small details, such as the leaves and small branches on the tree models. Also, MLFMM captures small details for electrically large problems without requiring too many computational resources. The FEKO simulated results of the measured 19-inch PEC sphere provides an excellent example of the fidelity of the MLFMM solver. Also, the symmetrical tree simulations were solved with MLFMM and more plot details were captured. As a result of this preliminary validation work, various FOPEN scene scenarios with realistic tree models were simulated with MLFMM and results of these simulations and details of this FOPEN research are found in [4] and [5].

REFERENCES

[1] M. E. Davis, Foliage penetration radar: Detection and characterization of objects under trees, Raleigh, NC: SciTech Publishing Inc., 2011.

[2] H. Hellsten, Meter-wave synthetic aperture radar for concealed object detection, Boston, MA: Artech House, 2017.

[3] S. I. Tsunoda, F. Pace, J. Stence, M. Woodring, W. H. Hensley, A. W. Doerry and B. C. Walker, "Lynx: a high-resolution synthetic aperture radar," *SPIE Aerosense,* vol. 3704, pp. 1 - 8, 1999.

[4] M. R. Jaramillo, A. W. Doerry and C. G. Christodoulou, "Modeling tree foliage for microwave radar transparency study," SAND Report SAND2020-14314, December 2020.

[5] M. R. Jaramillo, *Computational electromagnetic modeling (CEM) of foliage penetration (FOPEN),* Ph.D. dissertation. Electrical and Computer Engineering (ECE) Department. The University of New Mexico (UNM), Albuquerque, NM, 2021.

[6] M. R. Jaramillo, A. W. Doerry and C. G. Christodoulou, "Impulse Response Results from FOPEN Simulations," SAND Report SAND2021-6551, May 2021.

[7] M. R. Jaramillo, C. G. Christodoulou, S. Baua and J. Pennington, "Simulation study of high-fidelity foliage penetration (FOPEN) at Ku-band frequency," Altair White Paper, May 17, 2021.

[8] "Altair FEKO," [Online]. Available: https://www.altair.com/feko/.

[9] Y. W. Gu and M. S. Tong, "A volume-element-free scheme for solving volume integral equations," *2011 IEEE International Symposium on Antennas and Propagation (APSURSI),* pp. 205 - 207, 2011.

[10] L. J. Jiang and W. C. Chew, "A mixed-form fast multiple algorithm," *IEEE Transactions on Antennas and Propagation,* pp. 4145 - 4156, 2006.

[11] E. Ubeda, J. M. Tamayo and J. M. Rius, "Stable discretization of the electric-magnetic field integral equation with the Taylor-orthogonal basis functions," *IEEE Transactions on Antennas and Propagation,* pp. 2466 - 2470, 2013.

[12] P. Hamel, J. Adam, G. Kubicke and P. Pouliguen, "An improved hybridization technique of geometrical optics physical optics," *2012 15 International Symposium on Antenna Technology and Applied Electromagnetics,* pp. 1 - 6, 2012.

[13] F. Weinmann, "PO/PTD ray tracing for arbitrary metallic and dielectric objects," *2006 First European Conference on Antennas and Propagation,* pp. 1 -5, November 2006.

[14] L. Yuan, B. Wang, W. Gao, Y. Xu, X. Wang and Q. Wu, "An effective methodology to design scale model for magnetic absorbing coating based on ORL," *Results in Physics,* vol. 7, pp. 1698 - 1704, 2017.

[15] A. W. Doerry and B. Brock, "Radar cross section of triangular trihedral reflector with extended bottom plate," SAND Report SAND2009-2993, June 2009.

[16] Y. He, S. -. Y. He, Y. -. H. Zhang, G. -. J. Wen, D. -. F. Yu and G. -. Q. Zhu, "A forward approach to establish parametric scattering center models for known complex radar targets applied to SAR ATR," *IEEE Transactions on Antennas and Propagation,* vol. 62, no. 12, pp. 6192 - 6205, 2014.

[17] C. Pena-Caballero, E. Cantu, J. Rodriguez, A. Gonzales, O. Castellanos, A. Cantu, M. Strait, J. Son and D. Kim, "A multiple radar approach for automatic target recognition of aircraft using inverse synthetic aperture radar," *2018 1st International Conference on Data Intelligence and Security (ICDIS),* pp. 24 - 31, April 2018.

[18] G. O. Glentis, K. Zhao, A. Jakobsson and J. Li, "Non-parametric high-resolution SAR imaging," *IEEE Transactions on Signal Processing,* vol. 61, pp. 1614 - 1624, April 2013.

[19] M. A. Karam, A. K. Fung, R. H. Lang and N. S. Chauhan, "A microwave scattering model for layered vegetation," *IEEE Transactions on Geoscience and Remote Sensing,* vol. 30, no. 4, pp. 767 - 784, July 1992.

[20] F. T. Ulaby and M. A. El-Rayes, "Microwave dielectric spectrum of vegetation - part II: dual-dispersion model," *IEEE Transaction on Geoscience and Remote Sensing,* Vols. GE-25, no. 5, pp. 550 - 557, September 1987.

[21] D. Liao and T. Dogaru, "Large-scale, full-wave scattering phenomenology characterization of realistic trees," *2015 IEEE International Symposium on Antennas and Propagation & USNC/URSI National Radio Science Meeting,* pp. 592 - 593, July 2015.

DISTRIBUTION

Email—Internal

Name	Org.	Sandia Email Address
Technical Library	01977	sanddocs@sandia.gov

Email—External (encrypt for OUO)

Name	Company Email Address	Company Name
Christos Christodoulou	christos@unm.edu	The University of New Mexico
John Fanelle	John.Fanelle@ga-asi.com	General Atomics – ASI

This page left blank

This page left blank

Sandia National Laboratories

Sandia National Laboratories is a multimission laboratory managed and operated by National Technology & Engineering Solutions of Sandia LLC, a wholly owned subsidiary of Honeywell International Inc. for the U.S. Department of Energy's National Nuclear Security Administration under contract DE-NA0003525.